INFORMATION TO USERS

This manuscript has been reproduced from the microfilm master. UMI films the text directly from the original or copy submitted. Thus, some thesis and dissertation copies are in typewriter face, while others may be from any type of computer printer.

The quality of this reproduction is dependent upon the quality of the copy submitted. Broken or indistinct print, colored or poor quality illustrations and photographs, print bleedthrough, substandard margins, and improper alignment can adversely affect reproduction.

In the unlikely event that the author did not send UMI a complete manuscript and there are missing pages, these will be noted. Also, if unauthorized copyright material had to be removed, a note will indicate the deletion.

Oversize materials (e.g., maps, drawings, charts) are reproduced by sectioning the original, beginning at the upper left-hand corner and continuing from left to right in equal sections with small overlaps.

Photographs included in the original manuscript have been reproduced xerographically in this copy. Higher quality 6" x 9" black and white photographic prints are available for any photographs or illustrations appearing in this copy for an additional charge. Contact UMI directly to order.

Bell & Howell Information and Learning
300 North Zeeb Road, Ann Arbor, MI 48106-1346 USA

UMI®
800-521-0600

THREE-DIMENSIONAL MEASUREMENT AND VISUALISATION OF HUMAN LUMBAR KINEMATICS

by

Richard K. Rubin, BEng

A thesis submitted in partial fulfilment of the requirements for the degree of

Master of Biomedical Engineering

McGill University, Montreal

August, 1997

National Library
of Canada

Acquisitions and
Bibliographic Services

395 Wellington Street
Ottawa ON K1A 0N4
Canada

Bibliothèque nationale
du Canada

Acquisitions et
services bibliographiques

395, rue Wellington
Ottawa ON K1A 0N4
Canada

Your file Votre référence

Our file Notre référence

0-612-44038-9

Canada

McGill University, Montreal

THREE-DIMENSIONAL MEASUREMENT AND VISUALISATION OF HUMAN LUMBAR KINEMATICS

by Richard K. Rubin, BEng

Supervisors:
Terry Peters, PhD
Dept. of Biomedical Engineering

Max Aebi, MD
Dept. of Experimental Surgery

Abstract

This thesis describes a system to record and visualise *in-vivo* human lumbar spinal kinematics. As well, an extensive method to quantify the system's accuracy and reliability is detailed within. A data acquisition system measures lumbar motion associated with exercises similar to daily activities (gait, ranging, and load lifting). This involves a minimally invasive procedure to insert pins into three spinous processes of the lumbar vertebrae. Three-dimensional electromagnetic position sensors are attached to these pins and stereo radiographs provide the calibration offsets necessary for the calculation of spinal segmental motion from the sensor data. Analysis software was written to aid researchers in extracting descriptive statistics and by displaying 2-D graphs of the segmental motion. As an adjunct to the analysis software, a method was developed to visualise the subject's kinematics using 3-D computer animation. This requires the subject to undergo magnetic resonance volume scans which yields vertebral surface data. This data and the previously acquired kinematics from the same person is combined through computer animation resulting in an intuitive visualisation of their spine's motion.

Resumé

Cette thèse décrit un système d'enregistrement et de visualisation des mouvements de la colonne lombaire in vivo chez l'homme. La précision et la confiance de cette méthode ont été quantifiées d'une manière approfondie. Un système de capture des données mesure les mouvements lombaires durant des exercices qui ressemblent aux activités quotidiennes (marche, rayon d'action, levée des poids). Pour réaliser ces mesures, une procédure légèrement invasive permettait le placement de trois tiges au niveau des processus épineux des vertèbres lombaires. Des détecteurs de positions électromagnétiques tridimensionnels sont attachés sur ces tiges. Des radiographies en stéréo fournissaient le décalage nécessaire pour calculer les mouvements segmentaires à partir des données obtenues par les détecteurs. Un logiciel d'analyse a été écrit pour aider les chercheurs à extraire les statistiques descriptives ainsi que visualiser les mouvements segmentaires sous forme de graphiques bidimensionnels. Une méthode pour visualiser les mouvements lombaires tridimensionnels avec l'aide d'animation informatisée a été également développée. Pour appliquer celle-ci les sujets ont dû subir un examen à la résonance magnétique qui permettait d'obtenir des images volumétriques de leurs colonnes lombaires. Les contours des surfaces vertébrales ont été extraits à partir de ces images. Les contours ont été combinés au moyen d'animation informatisée avec les données des mouvements acquis chez le même sujet. Ceci permettait la visualisation intuitive des mouvements lombaires.

Preface

This thesis documents original work of the author as partial fulfilment of the degree of Master of Biomedical Engineering, McGill University, Montreal, Canada. Research was performed at the McGill Orthopaedic Research Laboratory at the Royal Victoria hospital (Montreal) and in collaboration with the Brain Imaging Centre at the Montreal Neurological Institute (Montreal).

Included with the submission is one VHS video tape illustrating the results of the three-dimensional computer visualization. However, the author authorizes reproduction of this thesis by the department without the inclusion of the video tape.

The thesis is arranged as follows: Chapter 1 introduces the project and the motivation for its undertaking, surveys previous related studies and outlines the thesis objectives. Background information is provided in Chapter 2, which touches upon the major topics related to this project. Chapter 3 describes the data acquisition system for recording segmental kinematics and the calibration method used to validate it. The MR scanning protocol and the data conversion and transfer method is described in Chapter 4. Chapter 5 details the analysis and visualisation system which was developed to study the results from the segmental motion measurements. Chapters 6 and 7 follow with a presentation of the project's results and a discussion and conclusions based upon them.

Original Contributions

The original contributions of this thesis are the following:

- Improvement upon the previous methods to study human lumbar kinematics by measuring three-dimensional motion of healthy subjects *in-vivo*.

- Design and development of a three-dimensional data acquisition system suitable for *in-vivo* use on humans while satisfying all design requirements.

- Validation of the Fastrak electromagnetic tracking system for dynamic relative motion.

- Development of an intuitive user interface to manage the experimental procedure and resulting data.

- Creation of a software library and interface to analyse and visualize experimental data including two-dimensional graphs and three-dimensional computer animation.

Publications Resulting from this Work

The following conference presentations and papers are a result of the work described in this thesis:

Journal Papers:

Steffen T., Rubin R.K., Baramki H.G., Antoniou J., Marchesi D., Aebi M., "A New Technique for Measuring Lumbar Segmental Motion In-vivo. Method, Accuracy, and Preliminary Results," Spine 1997 Jan. 15;22(2):156-66

Oral Presentations

Steffen T., Baramki H.G., Rubin R., Antoniou J., Marchesi D., Aebi M. "Invasive Direct Measurement of Lumbar Segmental Kinematics." Annual Meeting, Canadian Orthopaedic Research Society, Halifax, June 1995.

Steffen T., Baramki H.G., Rubin R., Antoniou J., Beckman L., Marchesi D., Aebi M.. "Les amplitudes de mouvement et les caracteristiques de mouvement coule d'un segment lombaire mesures in-vivo." XXV Réunion Annuelle de la Société de la Scoliose du Québec, May 1995.

Steffen T., Baramki H.G., Rubin R., Antoniou J., Marchesi D., Aebi M. "*In Vivo* Measurement of the L3/L4 Segmental Motion Patterns in the Upright, Flexed, and Extended Positions." 42nd Annual Meeting, Orthopaedic Research Society, Atlanta, GA, February 1996.

Steffen T., Baramki H., Rubin R., Marchesi D., Aebi M.. "Dynamic Three Dimensional Lumbar Segmental Motion Patterns Measured in Healthy Subjects." 7th European Spine Society Meeting, Zuerich, October 1996.

Steffen T., H. Baramki, Rubin R., Marchesi D., Aebi M., "Lumbar Spinal Motion During Walking and Running." 26th Annual Meeting of the Quebec Scoliosis Society, Montreal, QC, May 1996.

Rubin R., Steffen T., Peters T., Aebi M., "3-D Computer Animation of Spinal Segmental Kinematics." 27th Annual Meeting of the Quebec Scoliosis Society, Hull, QC, May 1997.

Poster Presentations

Steffen T., Rubin R., Antoniou J., Baramki H., Marchesi D., Aebi M., "A new Method to Record *In-Vivo* Kinematics in the Human Lumbar Motion Segment." 41st Annual Meeting, Orthopaedic Research Society, Orlando, FL, February 1995.

Acknowledgements

I would like to acknowledge the efforts of all the members of the Orthopaedic Research Laboratory. This lab has a truly team oriented multi-disciplinary approach to its research and definitive lines cannot be drawn concerning contributions to a project spanning three years. However, certain individuals do merit specific mention as I am indebted to them for their input and guidance and I would like to thank them greatly. Dr. Thomas Steffen's scientific contributions filled in many gaps in my knowledge and we collaborated closely throughout the project's duration. His vision, enthusiasm and devotion to research is inspiring, and without which, this project would not exist. Lorne Beckman was responsible for engineering the strain gauge mounted pins and he also contributed to the assemblage of the analog data acquisition electronics. Aejaz Zahid provided the pin-deformation models included in the appendix. Dr. Max Aebi not only provided clinical input and leadership but he also shared the responsibility of inserting the pins into the subjects with Dr. Dante Marchesi.

As well, I would like to thank Dr. Terry Peters of the Montreal Neurological Institute for his help concerning medical imaging issues and for his supervision and editorial contribution.

Thanks are also in order for Dr. Hani Baramki for translating my abstract into French on such short notice.

Table of Contents

ABSTRACT i

RESUMÉ ii

PREFACE iii

ORIGINAL CONTRIBUTIONS iii

PUBLICATIONS RESULTING FROM THIS WORK iv

ACKNOWLEDGEMENTS vi

TABLE OF CONTENTS vii

TABLE OF FIGURES ix

1. INTRODUCTION 1

1.1 MOTIVATION 1
1.2 SURVEY OF PREVIOUS WORK 2
1.2.1 Direct Measurement Techniques *3*
1.2.2 Imaging Measurement Techniques *3*
1.3 THESIS OBJECTIVES 4

2. BACKGROUND 6

2.1 FUNCTION OF THE SPINE 6
2.1.1 Introduction: *6*
2.1.2 The Vertebrae: *7*
2.1.3 Co-ordinate System of the Vertebra *9*
2.2 ELECTROMAGNETIC POSITION TRACKING DEVICE 9
2.3 COMPUTER GRAPHICS 12
2.3.1 Introduction: *12*
2.3.2 The Quest for Visual Realism: *13*
2.3.3 Attributes of Realism: *13*
2.4 MAGNETIC RESONANCE IMAGING 14
2.4.1 Introduction: *14*
2.4.2 Nuclear Magnetic Resonance: *15*
2.4.3 Imaging Cycle: *20*
2.4.4 Tissue Contrast: *22*
2.4.5 Spatial Encoding: *23*
2.4.6 Image Reconstruction: *28*
2.4.7 Image Quality: *28*
2.4.8 Biologic Effects and Safety Considerations: *29*

3. SEGMENTAL KINEMATICS MEASUREMENT SYSTEM 30

3.1 SYSTEM REQUIREMENTS AND OVERVIEW 30
3.2 KINEMATIC DATA ACQUISITION 31
3.2.1 Instrumentation and Experimental Set-up *31*
3.2.2 Data Acquisition Hardware and Interfacing *35*
3.2.3 Software Design *38*
3.3 CALIBRATION 43
3.3.1 Calibration Attachment *44*
3.3.2 Computer Assisted X-Ray Analysis *45*
3.3.3 X-Ray Measurements And CST Calculation *46*

3.4 DATA POST-PROCESSING 50
3.5 VALIDATION METHOD 52
3.5.1 System Reliability *52*

4. MRI ACQUISITION **54**

4.1 DATA TRANSFER AND CONVERSION 55

5. KINEMATICS VISUALIZATION SYSTEM **56**

5.1 2D VISUALIZATION AND QUANTITATIVE ANALYSIS SOFTWARE 56
5.1.1 Software Functionality – Overview *56*
5.2 3D MR DATA ANIMATION 58
5.2.1 Programming Environment *58*
5.2.2 Segmentation *58*
5.2.3 Geometry Rendering *63*
5.2.4 Animation *64*

6. RESULTS **66**

6.1 VALIDATION OF THE KINEMATIC DATA ACQUISITION SYSTEM 66
6.1.1 System Accuracy *66*
6.1.2 System Reliability *68*
6.1.3 Comparison To Cineradiography *70*
6.2 COMPUTER ANIMATION 70
6.2.1 Explanation of Video *71*

7. DISCUSSION & CONCLUSION **72**

8. APPENDIX **74**

8.1 ERRORS DUE TO PIN DEFORMATION 74

9. REFERENCES **78**

10. GLOSSARY **84**

Table of Figures

FIGURE 1-1 - VERTEBRAL COLUMN 6
FIGURE 2-1 - LUMBAR VERTEBRA, SUPERIOR VIEW 7
FIGURE 2-2 - LUMBAR SEGMENT, POSTERIOR VIEW 8
FIGURE 2-3 - BEFORE THE RF PULSE: RANDOM PRECESSION ABOUT THE MAIN MAGNETIC FIELD, AND THE NET MAGNETISATION, M, IS IN THE SAME DIRECTION 17
FIGURE 2-4 - AFTER THE RF PULSE: PHASIC PRECESSION OF NUCLEAR MOMENTS RESULTS IN A NET MAGNETIC MOMENT WITH A TRANSVERSE COMPONENT 18
FIGURE 2-5 - T1 OR LONGITUDINAL RELAXATION 19
FIGURE 2-6 - T2 OR TRANSVERSE RELAXATION 20
FIGURE 2-7 - SPIN ECHO IMAGING CYCLE 21
FIGURE 2-8 - ORTHOGONAL MAGNETIC FIELD GRADIENTS 24
FIGURE 2-9 - SLICE SELECTION DURING SELECTIVE EXCITATION 25
FIGURE 2-10 - SPIN ECHO PULSE SEQUENCE 27
FIGURE 3-1 - SECOND GENERATION PIN-MOUNTS: SHOWN ON LEFT, FASTRAK SENSOR (2) ATTACHED TO PIN-MOUNT. THE MOUNT IS FIXED TO A PIN (A) USING A SET-SCREW (B). ON RIGHT, CALIBRATION ATTACHMENT AND METAL BEARINGS (D) WHICH SLIDES INTO GROVE OF PIN-MOUNT (C). 33
FIGURE 3-2 - THIRD GENERATION PIN-MOUNTS: THREE PIN-MOUNTS FIXED TO THE SUBJECT'S PINS IN A STAGGERED LATERAL CONFIGURATION. A CALIBRATION ATTACHMENT IS SHOWN IN THE SURGEON'S HAND, READY TO SLIDE ONTO A PIN-MOUNT 34
FIGURE 3-3 - SUBJECT WEARING EXPERIMENTAL MONTAGE: SHOWN ARE THE THREE FASTRAK SENSORS ATTACHED TO THE SUBJECT'S PINS BY THE THIRD GENERATION PIN-MOUNTS. THE TRANSMITTER IS THE BLACK CUBE IN THE CENTRE OF THE HARNESS 35
FIGURE 3-4 - STRAIN GAUGE AUGMENTED PINS: TWO STRAIN GAUGE AUGMENTED PINS READY FOR INSERTION. 36
FIGURE 3-5 - FOOT SENSORS FOR GAIT CORRELATION 37
FIGURE 3-6 - *IN-VIVO* MAIN USER INTERFACE 39
FIGURE 3-7 - ACQUISITION SEQUENCE FLOW CHART: THE USER INTERACTS ONLY WITH THE MASTER COMPUTER AND IT SENDS SIGNALS TO THE SLAVE VIA TCP/IP. 42
FIGURE 3-8 - CALIBRATION ATTACHMENTS 44
FIGURE 3-9 - A/P RADIOGRAPH 45
FIGURE 3-10 - LATERAL RADIOGRAPH 45
FIGURE 3-11 - A/P RADIOGRAPH SCHEMATIC SHOWING LANDMARKS 46
FIGURE 3-12 - LATERAL RADIOGRAPH SCHEMATIC SHOWING LANDMARKS 47
FIGURE 3-13 - RELATIVE SEGMENTAL MOTION CSTS: THE EQUATION AT THE BOTTOM OF THE FIGURE IS EVALUATED DURING POST-PROCESSING FOR EACH KINEMATIC SAMPLE INSTANCE 51
FIGURE 5-1 - NORMALISATION ANALYSIS MODULE: GRAPHICAL USER INTERFACE 57
FIGURE 5-2 - ANTERIOR MRI SLICE OF LUMBAR REGION 60
FIGURE 5-3 - MANUAL TRACING USER INTERFACE: THE USER TRACES THE CONTOURS ON EACH SLICE (LEFT) AND THE CORRESPONDING FILLED REGION IS SHOWN (MIDDLE) AND THE CURRENT 3-D OBJECT (RIGHT). 62
FIGURE 5-4 - AVS NETWORK FOR MANUAL TRACING AND ISO-SURFACE FUNCTIONS 63
FIGURE 5-5 - RENDERED L3/L4 VERTEBRAL SEGMENT 64
TABLE 6-1 - DYNAMIC RMS ERROR FOR ANGULAR MOTION 67
TABLE 6-2 - DYNAMIC RMS ERROR FOR LINEAR MOTION 68
TABLE 6-3 - PIN BENDING IN THE CRANIO-CAUDAL DIRECTION DURING VARIOUS RANGING EXERCISES IN FOUR SUBJECTS: CALCULATED MAXIMAL ANGULAR AND LINEAR ERRORS FOR SEGMENTAL MOTION MEASUREMENTS USING TWO DIFFERENT BEAM-BENDING MODELS (APPENDIX). 69
FIGURE 8-1 & 8-2 - PIN DEFORMATION SCHEMATICS FOR THE POINT FORCE MODEL (TOP) AND THE UNIFORMLY DISTRIBUTED LOAD MODEL (BOTTOM) 77

1. Introduction

1.1 Motivation

Biomechanical studies of the spine are motivated by the widespread impact of low back disorders (LBD) upon modern society. The importance of studying, understanding and managing LBDs can be seen by considering their impact on the economy and the health-care system. LBD is one of the leading causes for work loss in the western world with an associated loss in work time estimated at 93 million days per year in the United States alone[1, 2]. LBD affects 70-80 percent of the population at some time during their lives[3] and each year 5% of adults experience LBD[4] resulting in direct health-care costs and insurance payments estimated as high as 80 billion dollars annually in the United States[5,6] .

In spite of the efforts to better understand the natural history of spinal disorders, the etiology of LBD remains unclear, especially the onset of idiopathic low back pain and its potential as a chronic disease. Precise descriptions of morphological changes that produce or accompany spinal disorders exist, but there is a lack of comprehensive methods to evaluate the mechanical function of a spine *in-vivo*. Mechanical function is described in terms of kinematics and the associated forces on the spinal structures. *In-vivo* measurement techniques to estimate forces are imprecise (e.g., electromyograms combined with mathematical models). Therefore, clinical studies of spinal biomechanics often focus on kinematics only.

Since the spine's morphology and mechanical behaviour are co-dependant, a preoperative test of the spine's kinematics may help the surgeon to choose the optimal method to restore normal function. Post-treatment tests could evaluate a procedure's effectiveness and may assess long-term effects of the mechanical alterations induced in surgery. Kinematic studies comparing healthy versus pathological spines may further the understanding of different spinal disorders and their associated etiologies.

1.2 Survey of Previous Work

To study human spinal kinematics, the researcher must choose a model to observe. The choices can be broken down into animal and human models, and then subdivided into *in-vivo* and *in-vitro* subjects or specimens. The most "true to life" model is obviously an *in-vivo* study of living humans. This is due to the various limitations in both, animal and human cadaveric models. Since animal anatomy is quite different from human anatomy and since most animals are quadrupeds, the animal spine does not distribute loads the way a human spine would. Cadaveric studies lack the element of muscular control and the associated forces imparted on the spine by the surrounding muscles.

Previous studies to measure human spinal kinematics *in-vivo* can be grouped into two classes. Those that use direct measurement techniques with physical coupling between the sensors and vertebrae and those that use imaging techniques to 'view' the spine's motion. The former group requires some means of attaching a sensor to the spine, and vary in their level of invasiveness. The latter group uses some form of imaging modality, such as magnetic resonance imaging (MRI), computed tomography (CT) and ultrasound to image the spine.

1.2.1 Direct Measurement Techniques

An ideal, direct measurement method would be completely non-invasive and highly accurate in all six degrees of freedom (DOF). Unfortunately, such a method does not exist. Currently, the problem lies in the trade-off between invasiveness and accuracy. Invasive techniques bear a slightly increased risk for complications, may cause the subject discomfort and could possibly influence the spine's motion. However, as the technique becomes less invasive, it begins to suffer from poorer accuracy.

Clinical observation of the spine often employ easy to use, non-invasive goniometers to measure angles[7-9] . Goniometers provide gross measurements of the whole spine, but these are inaccurate and provide no information on segmental displacement[9-11] . Other authors have reported using skin mounted optical sensors[12-15] or electromagnetic sensors[16-19] . While the sensors themselves are more accurate than goniometers and they can track individual vertebrae, they are not rigidly attached to the vertebrae. The skin and underlying fascia are free to stretch and shift, especially in large range of motion (ROM) exercises, which cause the sensor and vertebrae to experience relative motion and degrade measurement accuracy[20-22] .

More invasive approaches have also been reported where Kirschner wires or Steinmann pins were inserted into the spinous processes and measurements were made using protractors[23-25] . These studies were limited to measuring axial rotation in fixed postures. Dynamic measurements by Kaigle et al. used a similar technique and a linked transducer to measure two-dimensional sagittal plane rigid-body motion[26] .

1.2.2 Imaging Measurement Techniques

Imaging methods are generally considered non-invasive, however some methods use ionising radiation (e.g., CT, plain x-ray and stereo radiography). Standard planar radiological methods[27-29] are the most simple. They only provide two-dimensional (2-D), static images (usually in end-ranges of motion) and the difficulty in identifying identical anatomical landmarks on multiple films makes them imprecise[30, 31].

Standard radiological methods can be improved: First, the dimension of time can be measured and second, three-dimensional (3-D) data can be acquired. Cineradiography allows measurement of 2-D kinematics for dynamic posture changes[12, 32], and stereo radiographic methods use two 2-D images acquired from different perspectives to calculate 3-D positions[33-35]. To improve the identification of identical landmarks from multiple views, small radio-dense markers can be embedded in the bone[36, 37] and/or some form of mathematical optimisation may be performed[38, 39].

CT or MR scanners house the subject inside a narrow cylindrical enclosure. Scans for studying spinal kinematics are restrictive due to the limited space available for altering a subject's posture and except for a small number of specialised units, suffer from the lack of gravity to physiologically load their spine.

1.3 Thesis Objectives

The goal of this project is to develop a computer-assisted technique to study lumbar spine kinematics *in-vivo* and present the results so that the complex, 3-D nature of the spine’s motion can be easily visualised and interpreted. The practical application resulting from this thesis will be a tool to measure, analyse and visualise the spine's kinematics. It is intended to be used by a variety of people (e.g., clinicians, technicians and engineers), therefore, the user interface should be simple and easy to use, yet provide full functionality.

The measurement sensors are required to have adequate resolution and accuracy (temporal and spatial) to record the small segmental motions (i.e., axial rotations and linear displacements) that occur during routine, everyday activities. Therefore, a realistic experimental set-up is needed to validate the method's accuracy and reliability.

Equally important to the collection of data is its presentation--the most obvious method being 2-D graphs for quantitative analysis of the motion patterns. Since the data are recorded and stored in binary, a minimum requirement would be to have a tool to translate the information into a human-readable format. Such a utility, capable of translating binary data files into ASCII tab-delimited spreadsheets, makes the data universal and easily imported into popular spreadsheet and statistical analysis programs. Much of the quantitative analysis is very repetitive, consequently, a tool to read the binary data, directly display 2-D graphs, and then automatically perform certain calculations (e.g., range of motion (ROM), maximum amplitude, curve smoothing or normalisation, etc.) would be an improvement over the need to always transfer the data to a spreadsheet first.

The best way to convey 3-D motion on a computer is through animated 3-D computer visualisation. To accomplish realistic 3-D animation, the kinematic data must be combined with a 3-D data set describing the surface of each vertebra. This requires each subject to undergo volume scanning to acquire vertebral surface information. MR is favoured over CT, solely because CT exposes the subject to radiation. This implies that, prior to scanning, a protocol to optimise image quality must be determined.

2. Background

2.1 Function Of The Spine

2.1.1 Introduction:

The spine is a complex structure of vertebrae, discs, and ligaments extending between the base of the skull, through the neck and trunk and ending at the pelvis. Its functions are to protect the spinal cord; to manage force distributions from the head and trunk to the pelvis; to stabilise head and trunk posture; and to allow movement. The entire spine can be looked upon as a single ball and joint socket with a large range of motion. This large range of motion is accomplished through a cascade of jointed vertebra which are able to translate and rotate about all three axes.

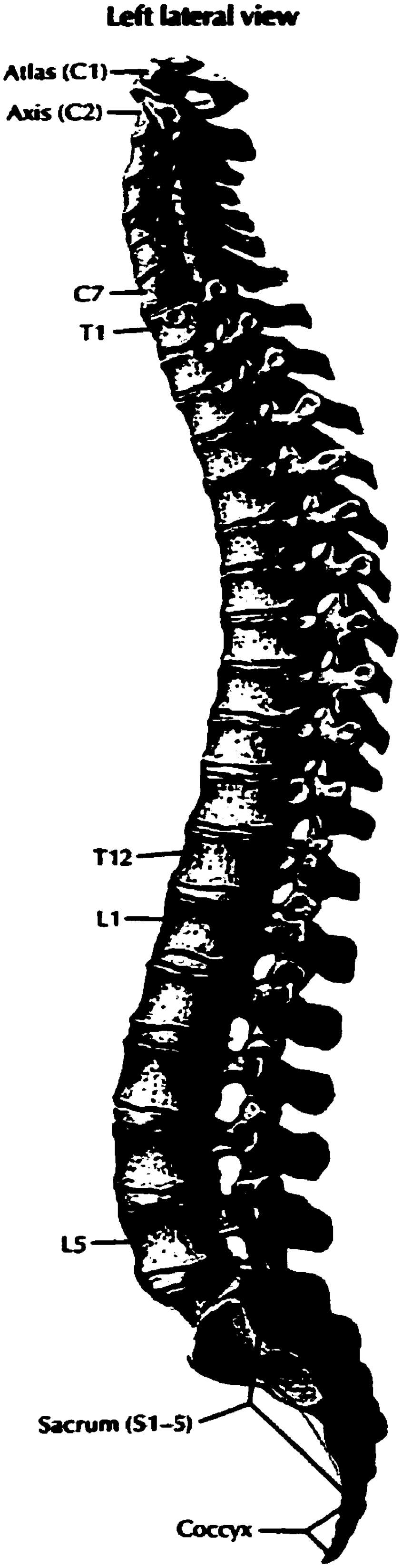

Figure 1-1 - Vertebral Column

The vertebral column usually consists of 33 vertebrae, arranged in five regions, but only 24 of them are moveable (7 cervical, 12 thoracic, and 5 lumbar). In adults, the five sacral vertebrae are fused to form the sacrum and the four coccygeal vertebrae are fused to form the coccyx. The seven upper-most vertebrae form the neck and are collectively referred to as the cervical spine. In this region, flexibility has been gained at the expense of stability. The cervical spine rests upon the thoracic spine, which is more rigid due to the rib cage and is less subject to injury than the more mobile cervical and lumbar spine regions. The largest vertebrae belong to the lumbar spine which carry the largest loads.

The movable vertebrae are connected by intervertebral discs (with the exception of the upper cervical spine), which play an important role in movements between the vertebrae and in absorbing shock transmitted up or down the vertebral column. The movable vertebrae are also connected to each other by paired, posterior facet joints between the articular processes and by strong anterior and posterior longitudinal ligaments. These ligaments extend the length of the vertebral column and attach to the intervertebral discs and vertebral bodies. These ligaments and joints generally prevent excessive movement of the vertebral column.

2.1.2 The Vertebrae:

The vertebral bodies make up approximately 75% of the length of the spine and the disc height contributes to the remaining length. The vertebral bodies are smallest at the top of the spine and gradually become larger as the sacrum is approached and then become progressively smaller toward the coccyx.

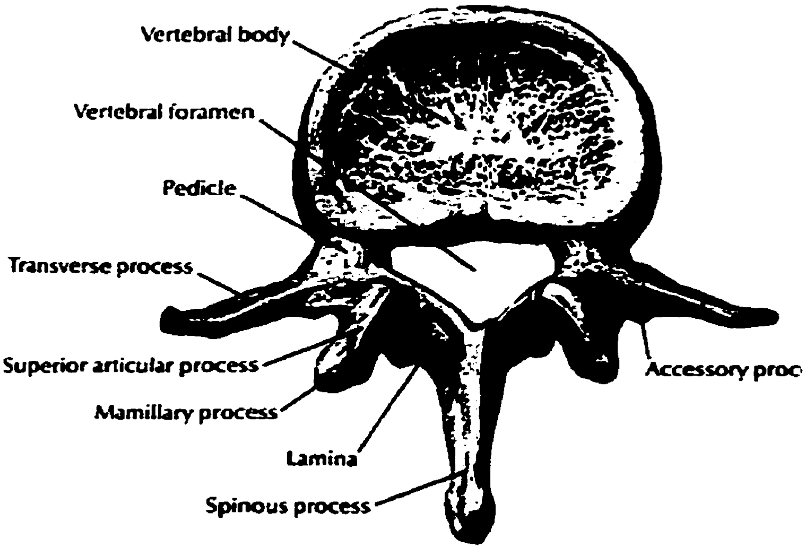

Figure 2-1 - Lumbar Vertebra, Superior View

A typical vertebra is composed of two parts, a body and a vertebral arch. The body is the large, heavy and anterior part which is characterised by its roughly cylindrical shape. Its function is to support weight. The superior and inferior surfaces of the body are rough and flat where they interface with the intervertebral discs. The vertebral arch attaches posteriorly to the body at two sites. It encloses the spinal chord and nerve roots, in a space called the vertebral foramen, and protects them from injury. The arch is formed by two short stout pedicles which project posteriorly from the body to meet with two broad flat laminae. The laminae join posteriorly to form the spinous process. Four articular processes and two transverse processes also stem from the vertebral arch. The spinous and transverse processes act as levers to increase the muscles' and ligaments' leverage on the vertebral column. The four articular processes project from the junctions of the pedicles and laminae. Two of the articular processes project superiorly and the other two project inferiorly and each process ends in an articular facet. Each vertebra's pair of superior and inferior facets articulates with those of the adjoining vertebrae to form a facet joint. The facet's surface is covered by hyaline cartilage and the joint is surrounded by an articular capsule which attaches to the articular edge of the processes.

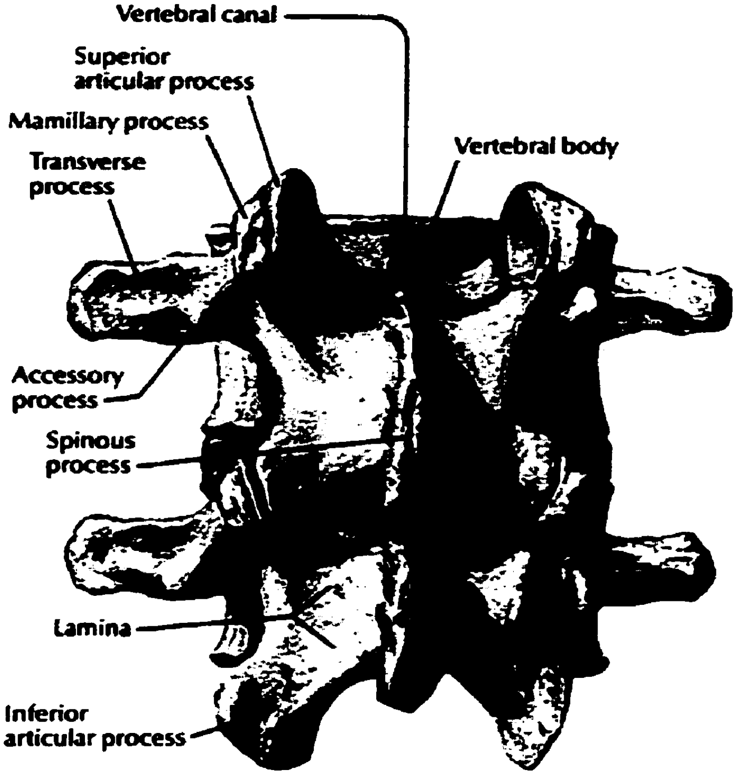

Figure 2-2 - Lumbar Segment, Posterior View

The shape and orientation of the facet surfaces determine their limitation on a vertebral segment's relative motion. For instance, the lumbar spine's facets are more aligned with the sagittal plane than the cervical spine's facets and therefore axial rotation is more limited in the lumbar spine. The range of motion of the vertebral column varies greatly from individual to individual, and with training this range can be extended considerably. The range of motion is limited by three factors: 1) the height and compressibility of the intervertebral discs, 2) the stiffness of the muscles and ligaments attached to the spine, and 3) the tension of the articular capsules of the facet joints. The relative segmental motion between two vertebrae is small, but the summation of these small displacements contribute to a substantial overall range of motion for the spine.

2.1.3 Co-ordinate System of the Vertebra

The movements of the spine can be described as displacements about an anatomical co-ordinate system. The right-handed co-ordinate system, as described by Panjabi [40], labels the normal to the sagittal plane as the x-axis (positive pointing left), the normal to the transverse plane as the y-axis (positive pointing superiorly) and the normal to the frontal plane as the z-axis (positive pointing anteriorly). Flexion and extension are described as rotation about the x-axis with flexion being positive. Axial rotation is angular rotation about the y-axis (rotation to the left is positive) and lateral bending is rotation about the x-axis (bending to the right is positive).

2.2 Electromagnetic Position Tracking Device

To completely describe a co-ordinate system relative to another in three dimensional space, one needs six orthogonal parameters, three of which describe the positional offset in the three co-ordinate axes between the two systems. The other three describe the orientation of one system relative to the other. Using Euler angles is one convenient way to describe this offset in orientation. Euler angles describe a series of rotational displacements about each of the three co-ordinate axes. The order is not commutative and the convention is to first rotate about the Z axis (Azimuth), then about the Y axis (Elevation) and finally about the X axis (Roll). Sometimes these rotations are referred to as Yaw, Pitch and Roll as well, but the order remains Z, Y, and X.

The position tracking device used for this project was the 3Space Fastrak (Polhemus, Colchester VT), consisting of a transmitter and four receivers. The transmitter creates an electromagnetic field using three coil antennae oriented in mutually orthogonal planes. The receivers sense the electromagnetic field created by the transmitter using a similar three coil receiving antennae construct. Polhemus also supplies the electronics to drive the transmitter and calculate the receivers' positions and orientations relative to the source. This information is then coded as positions and Euler angles in ASCII text or binary format which can be acquired by a computer through it's serial or GPIB port.

The coil antennae of the transmitter and receivers consist of fixed magnetic-dipoles. Exciting the transmitter coils creates a two-component near- and far-field. The far-field component's intensity is a function of loop size and excitation frequency and drops off as an inverse function of the distance ($1/r$). The near-field or quasi-static field is only proportional to the proximity to the source as an inverse function of the radius cubed ($1/r^3$). It is the near-field that is used for measurement purposes, and since it only dominates the far-field's intensity in close proximity to the transmitter, the maximum measurement distance between sensor and transmitter is limited to about 76 cm for optimum accuracy. This operational envelope can be expanded at the expense of measurement accuracy for greater radii.

To determine one receiver's position and orientation relative to the transmitter, each of the source's three coils is excited in sequence. Each excitation creates a magnetic dipole that is sensed by the three receiver coils. After all three transmitter coils have been energised, the electronics use the three sets of three measurements from the receiver to calculate it's position and orientation. There are always two solutions to the receiver's position, so only one half of the operational sphere about the transmitter gives unique results, therefore all receivers must remain in the same hemisphere.

The system's maximum sampling rate is 120 Hz, but the receivers are sampled sequentially so the actual sampling frequency per receiver is 120 Hz/*n*, where *n* is the number of active receivers. Therefore, when making receiver-to-receiver relative calculations, an interpolation is needed to estimate all the active receiver's positions at the same instant in time.

The static accuracy and resolution of the system was determined by Polhemus. The manufacturer defines the accuracy of the system to be the fractional error associated with a measurement, and the resolution to be the smallest amount of the quantity being measured that the instrument will detect. These two quantities are reported separately for both angular and positional measurements.

To calculate the angular resolution, the range of detectable values (0-360 degrees) is divided by the signal to noise ratio of the system. Polhemus reports this to be 0.025 degrees. Linear resolution is not solely a function of the S/N ratio, the distance separating receiver and transmitter is also a determining factor. Therefore, the linear resolution is reported as 0.0005 cm per cm of separation.

A statistical quantity is used to describe the accuracy of the system and is stated as a root mean squared (RMS) value. This statistical value incorporates error terms for linearity, repeatability, hysteresis, and drift. The linear static accuracy is quoted as 0.08 cm RMS, and the angular static accuracy is quoted as 0.15 degrees RMS. These RMS values are for all points within the optimal operating radius of 76 cm.

Since this system is based on the principles of electromagnetism, one confounding factor is the disturbance of the electromagnetic field due to the presence of ferrous materials in the near-field. For this reason, considerable effort was made to minimise the presence of ferrous materials in the vicinity of the Fastrak device. As well, since the complete elimination of conductive metal was not possible, all validation experiments and hence their quantitative results, include the error contribution of this disturbance.

2.3 Computer Graphics

2.3.1 Introduction:

Soon after the advent of the computer, computer graphics was recognised as an efficient method for man/machine communication. Unfortunately, there wasn't much growth in the field due to the high cost of the hardware required and the limited number of people with the technical skills needed to program computers, so computer graphics remained in its initial role as an interface to hard copy plotters and CRTs. This changed in the late 1970s with the proliferation of the personal computer into millions of homes. Companies like Xerox, Apple, IBM, and Commodore were selling affordable computers with bitmaped graphics, raster-scan displays, and easy-to-use applications. As computers became more powerful, the graphics became more sophisticated, and now computer graphics has found it's way into a rich diversity of fields such as engineering, medicine, science, business, entertainment, and art.

Computer graphics provides the most effective way for people to interact with computers. Our highly developed 2D and 3D pattern recognition abilities allow quick and efficient processing of pictorial data. This increases our ability to understand data, perceive trends, and visualise real or imaginary objects.

Time varying animation is becoming an important application of computer graphics and as processing power becomes more readily available, animation begins to assume an element of reality that rivals conventional film or video. The advantage of using a computer to create a dynamic scene is that the animated objects can be limited to exist solely in the computer's memory. Therefore, many systems or objects which couldn't otherwise have been *seen*, are readily visualised with the aid of a computer. Augmented reality is another application which overlays computer graphics on real-world scenes to convey more information than would normally have been available.

2.3.2 The Quest for Visual Realism:

An image can be judged for realism based on its ability to capture or simulate the effects of light's interaction with real objects. It should also be noted that a more realistic image is not always better--augmented reality being a prime example--so, exactly how much realism is required is a function of the application's goals.

The fundamental difficulty of producing a realistic image is the inherent complexity and richness of the real world. Therefore, the more realistic the image, the more complex the object model and, hence, the more computational time and memory required to render the scene (even the most powerful computers can take minutes to hours to render highly detailed and realistic images).

2.3.3 Attributes of Realism:

There are certain attributes of a real image that a computer can simulate to achieve realism. Since holographic displays are not readily available, most computers use a 2-D screen to display their rendered scene. Therefore, the 3-D world must projected onto a 2-D surface. The third dimension of depth can be conveyed using certain depth cueing techniques such as perspective, occlusion and clipping. If the viewing system is augmented with special eye-wear or head-gear for the user, stereo separation and parallax effects are possible, heightening the three dimensional effects.

Since there is more to creating a realistic image than conveying depth, surfaces must also be modelled by the way they reflect, absorb or transmit light. If the vertices and normals of a polygonal object's surfaces are specified, algorithms can interpolate the reflectance properties for the entire object's surface (i.e., Gouraud and Phong surface shading), textures can be mapped to the object and the object can affect the lighting characteristics of surrounding objects by casting shadows or reflecting light.

2.4 Magnetic Resonance Imaging

2.4.1 Introduction:

Since its development in the 1940's, nuclear magnetic resonance (NMR) has been used extensively to investigate the physical and chemical properties of matter. Damadian was among the first to suggest the use of NMR in medical diagnoses and Lauterbur published the first NMR image in 1972.

Magnetic resonance imaging (MRI) was introduced into clinical practice in 1981. Initially, it was predominantly directed toward diagnostic studies of the central nervous system (CNS) because the head is easier to image because of its small size and lack of respiratory or other physiologic motion. Since then, MRI has evolved at an explosive rate and now includes applications outside the CNS. Depiction of abnormalities of cancellous bone, joints, muscle, large blood vessels, fat, lymph nodes, liver, and spleen is also improving to the point where MRI has become an important and often the best diagnostic imaging modality available for these areas. In orthopaedics in particular, MR imaging of the spine and musculoskeletal system has particular advantages including high soft-tissue contrast resolution and discrimination, the ability to image in any plane, the absence of bone and some metal artefacts, and the use of non-ionising radiation. It should be noted that MR imaging reflects a proton population's concentration and environment. So, when speaking about imaging bone tissue, it is actually the lack of signal from bone that allows us to image it since it has relatively low water content compared with it's surroundings.

The dependence of MRI on at least seven parameters gives it unmatched flexibility and at the same time, great complexity. The magnetic resonance process is capable of producing images that are distinctly different from the images produced by other imaging modalities. A primary difference is that MR can selectively image several different tissue characteristics such as magnetic relaxation, proton density, and blood flow without using contrast medium.

Disadvantages of MRI include high cost, relatively long acquisition times, poor compact bone and calcium detail and patient discomfort due to claustrophobia and acoustic noise.

2.4.2 Nuclear Magnetic Resonance:

Certain materials take on resonant characteristics when placed in a magnetic field. They can thus absorb and re-radiate electromagnetic energy matching a harmonic which is typically in the radio frequency band (MHz). In MR imaging, it is this re-radiated energy that is sensed and imaged.

Any nucleus containing an odd number of protons or neutrons can be conceptualised as a small rotating magnet since electric charges in motion produce magnetic fields. The magnetic field can be characterised by a magnetic moment vector. When placed in an external magnetic field, this vector tends to align with the external field like a compass needle aligning in the earth's magnetic field. Due to the spinning motion of the nuclei, their moments do not align perfectly with the external field, rather, they precess about it's direction (much like spinning tops under the influence of gravity). The frequency of this precession is given by the Larmor equation:

$$\omega = \gamma \text{ x } B_O$$

where ω is the precessional (Larmor) frequency, γ is the gyromagnetic ratio, and B_O is the strength of the external field. Different types of nuclei have different gyromagnetic ratios. Because hydrogen nuclei possess the largest gyromagnetic ratio known (42.58 MHz/T), and hydrogen is extremely abundant in the human body, most medical MR imaging is based on the hydrogen nucleus.

2.4.2.1 Resonance:

The hydrogen nucleus, which consists of a single proton, can exist in either of two unequal energy states. The nucleus can either align itself in the direction of an external field (parallel) or against it (anti-parallel). The parallel state has a lower energy associated with it, and if all else were equal, the nuclei would tend to align themselves in the parallel state.

If all the magnetic moments were summed using vector addition, the result would be a bulk magnetisation vector. In the absence of an external magnetic field, the individual nuclear moments are randomly oriented and the bulk moment is zero. Once in an external field, there is a net increase of nuclei in the parallel state and hence the bulk magnetisation vector points in the direction of the external field. The population difference between parallel and anti-parallel states is 1-6 per 100,000 nuclei, and it depends on the number of protons in the external field, the field's strength, and is inversely proportional to temperature.

2.4.2.2 Effect of RF pulses:

If subjected to electromagnetic radiation of the proper frequency, the nuclei will make rapid transitions between the two states. This process is called resonance, where energy is absorbed and emitted. This tends to reduce the number of excess nuclei pointing in the direction of the external field, which reduces the bulk magnetisation vector in the direction of the external field.

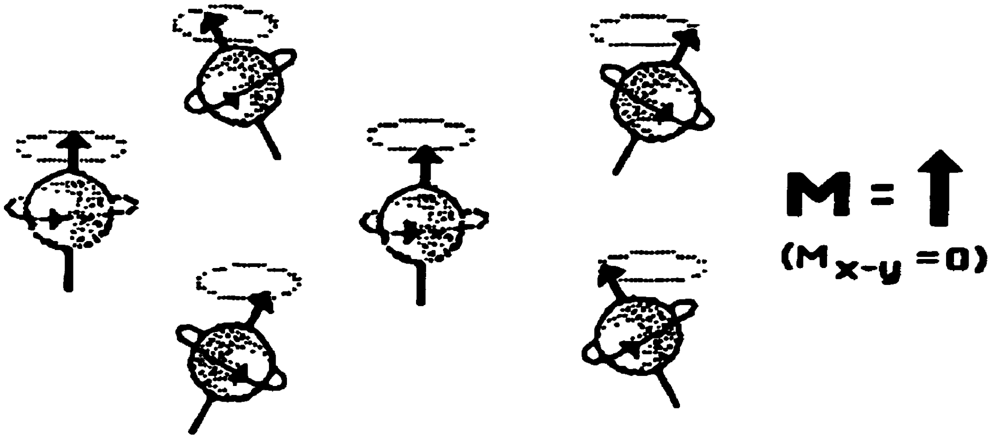

Figure 2-3 - Before the RF Pulse: Random precession about the main magnetic field, and the net magnetisation, M, is in the same direction.

Before the introduction of the RF pulse, the nuclei precess randomly about the direction of the main magnetic field. Therefore, the vector sum of the nuclear moments in the direction perpendicular to the main magnetic field (transverse X-Y plane) is zero . After the RF pulse, the moments precess in phase with one another, creating a vector component in the X-Y plane perpendicular to the main field. The net result of a RF pulse is to decrease the bulk magnetisation moment's magnitude in the z direction and to rotate the vector away from the z axis.

If the duration of the RF pulse is long enough, the bulk magnetisation moment will rotate 90 degrees and lie completely in the X-Y plane. This is known as a 90 degree RF pulse. After the RF pulse, the rotated bulk moment precesses about the main field direction at a rate proportional to the Larmor frequency. This rotating magnetic moment induces a current in a receiver coil known as the free-induction decay (FID) signal. The FID is an exponentially decaying sinusoid.

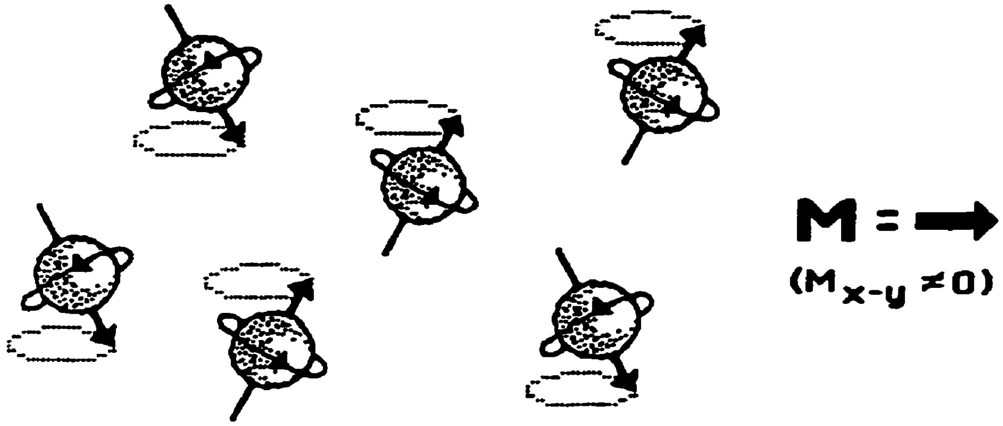

Figure 2-4 - After the RF Pulse: Phasic precession of nuclear moments results in a net magnetic moment with a transverse component.

2.4.2.3 T1 Relaxation:

Once the RF pulse ends, two important phenomena ensue. First the individual proton alignments begin to realign with the external field. This occurs because the parallel orientation is preferred due to its lower energy, and longitudinal magnetisation returns to static equilibrium. This is known as longitudinal or T1 relaxation. This process is a transfer of absorbed energy to the lattice. The rate at which this occurs is dependent on the molecular environment of the protons but in all cases, T1 relaxation follows a first order exponential equation.

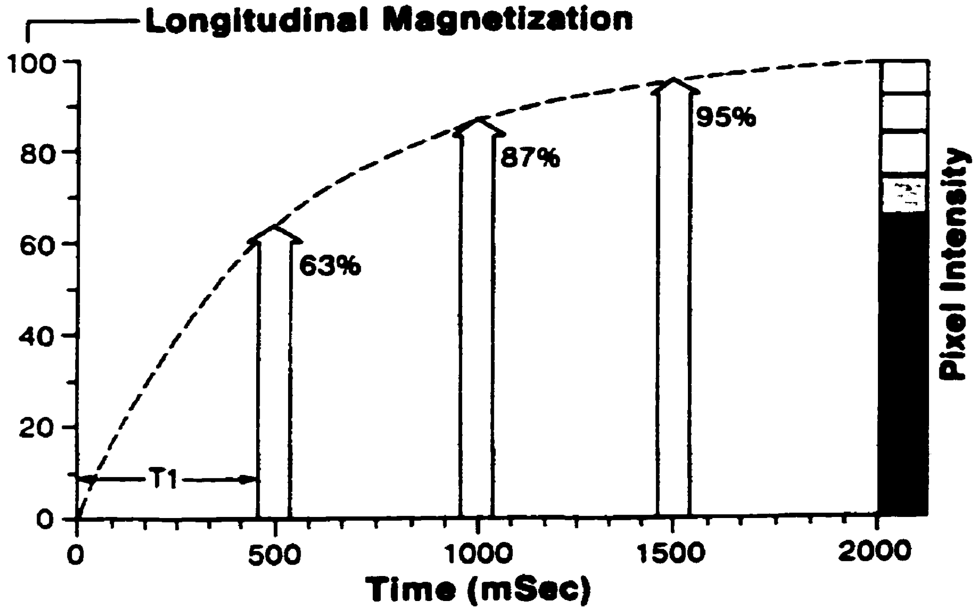

Figure 2-5 - T1 or Longitudinal Relaxation

T1 relaxation time is closely related to the molecular mobility of a tissue's constituent molecules, as well as magnetic field strength. Small molecules, such as water, have a relatively fast tumbling rate, and hence a long relaxation time. Similarly, large molecules like fats and proteins have slow tumbling rates, hence short T1 relaxation times. Therefore, fats and large molecules appear bright in a T1 weighted image and CSF appears dark.

2.4.2.4 T2 Relaxation:

The second phenomenon to occur after an RF pulse is known as T2 relaxation which is the result of the transverse component of the bulk moment returning to zero. This is caused by a loss of phase coherence in the precessing nuclear moments, due to sensed differences in the magnetic field. There are two main reasons for this difference: Static field inhomegeneity (T2*) and inherent local magnetic field differences due to the molecular environment (T2). If the external magnetic field was perfectly homogeneous, the T2* decay constant would equal that of T2.

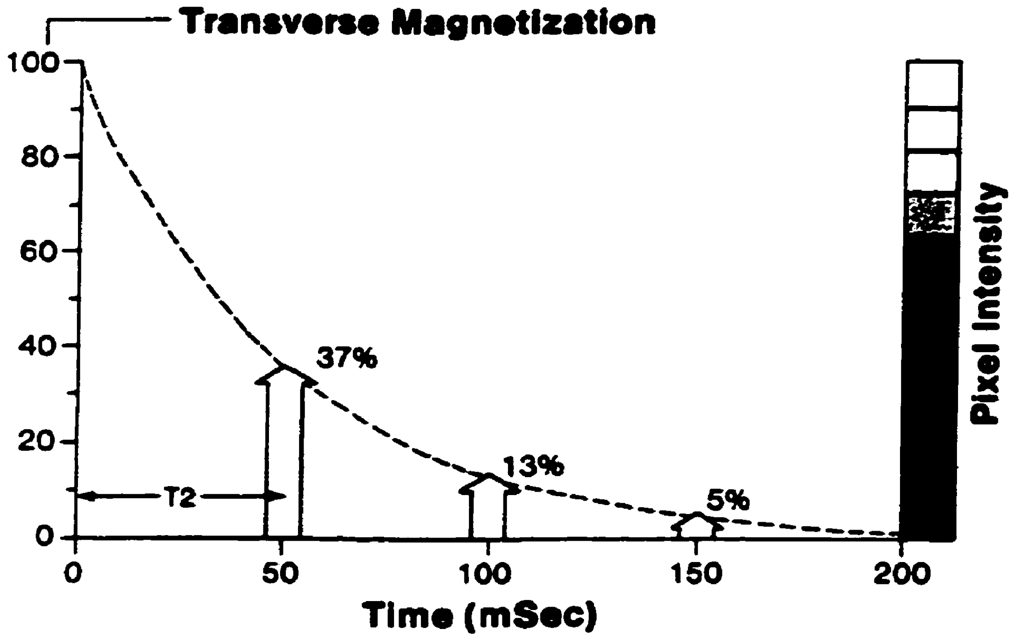

Figure 2-6 - T2 or Transverse Relaxation

T2, like T1, is tissue specific in the sense that different proton environments have highly characteristic T2 relaxation times. For pure water, T2 = T1, whereas in tissues, T1>>T2. Again, as in T1 relaxation, slower tumbling rates result in shorter T2 relaxation times (fat, proteins). An important factor, *in-vivo*, is the exchange between "free" water protons and water molecules that are bound to macromolecules. Thus, the relaxation time is a weighted average of bound and free water. Thus, tissues with low water content have short T2 relaxation times.

2.4.3 Imaging Cycle:

2.4.3.1 Spin-Echo:

Spin echo is the name of the process that uses an RF pulse rather than a gradient pulse to produce the echo event. It is also the name of one of the most clinically relevant imaging methods that uses spin-echo processes.

After a 90 degree excitation pulse, the nuclei are in-phase and the transverse magnetisation moment precesses about the main magnetic field's direction and a FID signal is produced. The FID signal is not used in spin-echo techniques but is used in gradient echo techniques (explained later). The decay of the FID is dominated by the inherent field inhomogeneity (T2*) and decays quickly due to the loss of phase coherence. In order to compensate for this decay which masks the T2 relaxation, a spin echo is generated. After significant FID decay (and phase coherence loss), a 180 degree pulse is used to flip the spins of the nuclei at time TE/2. Now the phase's of the faster spinning nuclei lag those of the slower ones. At time TE, the faster spinning nuclei catch up to the slower spinning nuclei and the transverse component of the bulk magnetisation re-appears because the nuclei are in phase again. Now the echo signals intensity is determined by the tissues T2 relaxation time because the tissue's dephasing is not reversible. This process can be repeated for the same initial excitation and is known as multi-echo imaging. TE is thus adjusted by varying the time between 90 and 180 degree pulses.

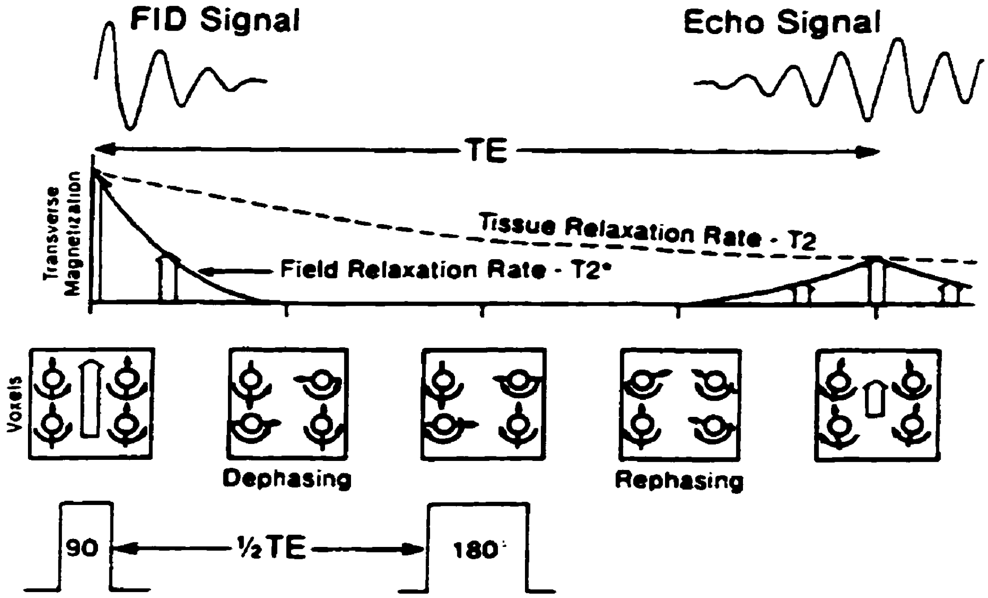

Figure 2-7 - Spin Echo Imaging Cycle

2.4.3.2 Gradient Echo:

It is possible to produce an echo event within the FID by applying a magnetic field gradient to the tissue. This also results in an RF signal from the tissue. The gradient echo technique first dephases the nuclei by turning on a gradient and then rephases them by reversing the direction of the gradient. This can be done during FID period or during a spin-echo event. This technique doesn't compensate for magnetic field inhomogeneity, and therefore the signal yields qualitative, rather than quantitative information about T2 and relative T2*. The image acquisition times are fast and produce a T1-weighted image with a high signal-to-noise ratio.

2.4.4 Tissue Contrast:

In MR imaging the usual procedure is to select one of the tissue characteristics and then adjust the imaging process so that it has good contrast sensitivity for that specific characteristic. Two important parameters are used in conventional spin-echo protocols to control contrast sensitivity: TR and TE.

TR is the repetition delay between excitation pulses which is the duration of the image acquisition cycle. TE is the time interval between the beginning of transverse relaxation and when the transverse magnetisation is measured. This is at the time of the "echo event," therefore TE is the time to echo.

2.4.4.1 Proton Density Weighted Image:

A proton density-weighted image is produced by selecting a relatively long TR value so that the image is taken in the latter portion of the longitudinal relaxation phase when tissue magnetisation is close to its maximum longitudinal value. The image intensity is then bright where protons are abundant. Usually this type of image is taken after 3 T1 decay constants (approx. 1,500 msec). This imaging modality is not as important as others since proton concentration is not a good contrast-generating parameter for soft tissue.

2.4.4.2 T1-Weighted Image:

With spin-echo protocols, TR is the parameter that determines T1 contrast sensitivity. The value of TR must be selected to correspond to a time where T1 contrast is significant between tissues. Choice of TR is a trade-off between good sensitivity and signal strength. Short TRs give good contrast but the longitudinal magnetisation hasn't had enough time to regain signal intensity. Normally, TR is chosen to be approximately one T1 decay constant for spin-echo imaging but it can be much lower for other imaging protocols. In a T1 weighted image, tissue with short T1 relaxation times show up bright (fats, macromolecules).

2.4.4.3 T2-Weighted Image:

Differences in T2 relaxation times can also be used to produce contrast in an image, and in this case the parameter that governs the contrast sensitivity is TE. At the echo event, transverse magnetisation levels are converted to RF signals. Again there is a trade-off between contrast and signal intensity, where longer TE is desirable for contrast maximisation but the longer TE, the smaller the transverse magnetisation.

Typical TE times are about 50 milliseconds. In a T2 weighted image, tissue with a short T2 relaxation times appear dark (white matter, muscle).

2.4.5 Spatial Encoding:

When imaging a subject in 3-D, the volume of interest is divided into a set of slices and then each slice is divided into rows and columns to form a matrix of individual tissue voxels. This is done by giving each voxel volume a specific frequency and phase encoding to separate it during image reconstruction.

Magnetic field gradients are used to give the RF signals their frequency and phase characteristics. The three sets of gradient coils are oriented so that gradients can be produced in three orthogonal directions (x, y, and z).

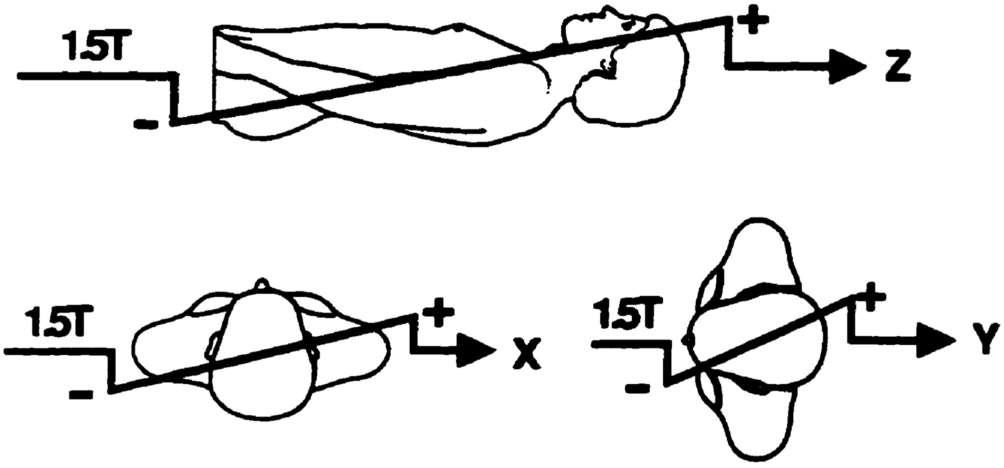

Figure 2-8 - Orthogonal Magnetic Field Gradients

There are two distinct methods used to divide a volume into voxel components: 1) selective excitation and 2) volume acquisition. Selective excitation creates slices during the acquisition phase, where volume acquisition acquires signals from a large volume and then slices the volume during the reconstruction process. Both methods use phase-encoding to divide the slices into voxels.

2.4.5.1 Selective Excitation:

During the RF excitation phase of selective excitation protocols, a linear magnetic field gradient is applied along one of the axes. Since the resonant frequency of a proton is directly proportional to the strength of the surrounding magnetic field, the gradient field has the effect of spatially encoding the volume by frequency in the direction of the gradient.

The RF excitation pulse has a narrow bandwidth compared to the range of resonant frequencies within the gradient field, consequently only a narrow slice of the volume is excited with this pulse. Therefore, the slice location and thickness can be controlled by adjusting the centre frequency and bandwidth of the RF pulse. The slice position is varied by changing the RF pulse's centre frequency (like tuning a radio to different channels). The slice thickness is determined by two factors: (1) the strength of the gradient, and (2) the range of frequencies in the RF pulse.

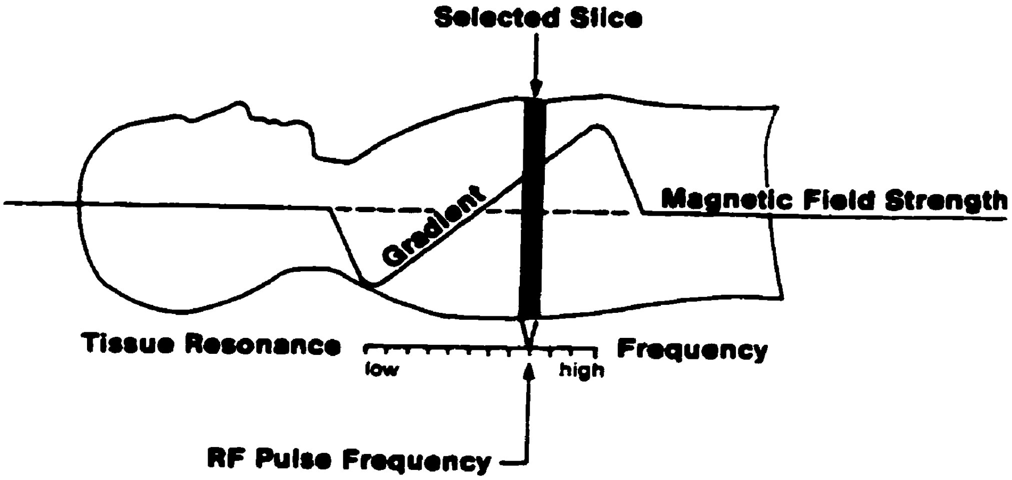

Figure 2-9 - Slice Selection during Selective Excitation

2.4.5.2 Phase Encoding:

Phase describes the time-shift between two periodic signals. Spatially varying phase differences, or phase encoding, is also used in MRI to resolve signal intensities in one or more dimensions.

A phase difference is created by temporarily changing the precession rate of the magnetisation moment of one voxel relative to another. This happens when two voxels are located in magnetic fields of different strengths, achieved by applying a field gradient across the subject.

Assume that all the voxels have the same amount of transverse magnetisation and that the magnetisation vectors are precessing in phase prior to phase encoding (i.e., no gradient is present). Applying a phase-encoding gradient causes the precession rates of some voxels to speed up and others to slow down and this change is proportion to the gradient strength and direction. The gradient is only on for a short time and when it shuts off, all the voxels return to the same precession rate, but now voxels along the gradient direction have a phase difference. When the echo event produces a signal from all the voxels simultaneously, the phase-encoding allows the signals from each voxel to be sorted out in the reconstruction process by using Fourier transforms.

During each pass through the imaging cycle, the phase-encoding is stepped through slightly different values by changing the gradient strength and the number of steps is equal to the number of voxels in the phase encoded direction.

2.4.5.3 Voxel Separation in the Slice:

The slice selection gradient is on during the RF excitation pulse (in selective excitation), limiting magnetic excitation and echo formation to the selected slice. Then a phase encoding gradient (orthogonal to the slice selection gradient) is turned on for a short period of time to phase-encode the first degree of freedom of the slice. Finally, during the echo event, a frequency-encoding gradient (orthogonal to the two previous gradients) is applied to spatially encode the final degree of freedom. This whole process is then repeated for each phase-encoding (number of pixels in the phase-encoding dimension). All the resulting signals for the slice are stored into one data set and a 2-D Fourier transform is used to convert the data into a 2-D image (see 2.4.6 - Image Reconstruction).

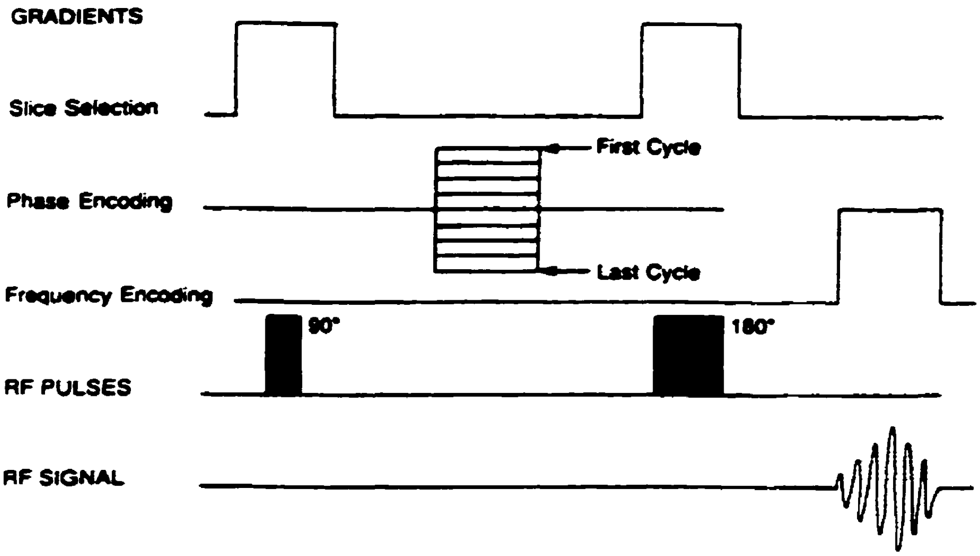

Figure 2-10 - Spin Echo Pulse Sequence

2.4.5.4 Slice Multiplexing:

Since we are usually interested in imaging a volume, multi-slice data are needed. The imaging process would be unacceptably long if each slice was imaged in series, but by taking advantage of the short duty cycle, slices can be imaged simultaneously. The process begins by applying an excitation pulse to one slice. Then, while that slice undergoes relaxation, the excitation pulse frequency is shifted to excite the next slice. This is done for the maximum number of slices that can be imaged during one TR interval. This is a significant efficiency gain when doing T2 weighted images (long TR).

A drawback to selective excitation is that, unlike the volume acquisition technique, it cannot produce thin contiguous slices.

2.4.5.5 Volume Acquisition:

With this method, no gradient is present when the RF pulse is applied. Since all tissue in the radiated volume is "tuned" to the same frequency, the whole volume is excited at once. Prior to the acquisition, the volume is phase-encoded to enable slice separation in the reconstruction phase. Phase encoding must be stepped through different values for each dimension corresponding to the number of slices to be created and for each line in every slice. This means a complete imaging cycle must be executed for each phase encoding.

Since the whole volume is excited for each gradient setting, there isn't the possibility for a performance gain obtained from slice multiplexing. Consequently, the acquisition times for volume acquisitions are much longer than those for selective excitation protocols. The advantages of volume scanning are that the phase-encoding process can generally produce thinner and more contiguous slices than selective excitation, and the signal to noise ratio improves by $\sqrt{n}$, where n is the number of "slices" in the 3-D volume.

2.4.6 Image Reconstruction:

Initially the signals that are acquired are not in the form of an image. Instead the data are in "k space" (i.e., the 2- or 3-dimensional Fourier transform of the image). In this space, the information is in the form of energy per spatial-frequency in two or threedimensions. A two- or three-dimensional Fourier transform is then required to transform the data into an image.

2.4.7 Image Quality:

There are three competing goals associated with imaging: 1) high spatial resolution; 2) low noise (high signal-to-noise); and 3) acquisition speed.

An artefact is something that appears in an image that is not a true representation of an object or structure. There is a variety of artefacts that can appear in MR images. Most are caused by errors in the spatial encoding of RF signals. Errors in phase-encoding are more common and larger, resulting in ghost images or bright streaks. Movement of body tissues and the flow of fluid during the image acquisition process is the most common source of artefacts. Serial averaging can help compensate for periodic or random motions. Flow compensation can be achieved with gradient moment nulling which involves applying a complex sequence of gradients during the scan sequence to produce the re-phasing of the signals from a flowing substance within each voxel.

2.4.8 Biologic Effects and Safety Considerations:

During the imaging process, a patient is subjected to three types of radiation: a static magnetic field, gradient or time-varying magnetic fields, and radio frequency electromagnetic radiation. Each of these forms of electromagnetic radiation can cause significant biologic effects if applied at sufficiently high exposure levels. Although numerous studies have been performed to identify potential biologic effects of MRI, none of these have determined the presence of any significant hazard but the data are still insufficient to assume absolute safety.

MRI scanners may interfere with the operation of electrical, magnetic or mechanic implants or devices. Ferromagnetic implants have the associated risks of (a) induced electrical currents, (b) heating, (c) possibility of dislodgement.

3. Segmental Kinematics Measurement System

3.1 System Requirements And Overview

The goal of this system is to measure a human subject's lumbar segmental kinematics *in-vivo*. The small vertebral movements that occur during various ranging exercises require the system to sample positions of several vertebrae fast and accurately. Therefore, the design tries to maximise measurement accuracy and temporal resolution while minimising invasiveness and economic cost.

The current configuration employs an electromagnetic position measurement system to sample the motion of the vertebrae by fixing sensors to pins drilled into the spinous processes. Following a calibration procedure to establish the sensor-vertebra relationship, positional data in six degrees of freedom are collected at a frequency high enough to measure spinal kinematics for exercises typical of daily activity.

The resulting system is flexible and scaleable with the ability to measure the kinematics of one or two adjacent motion segments simultaneously. Also, additional data may be collected via 16 analog input channels. The system design can be broken down into data acquisition, calibration, post-processing, and validation components which are further explained in the following sections.

3.2 Kinematic Data Acquisition

3.2.1 Instrumentation and Experimental Set-up

The experimental routine requires the subject to begin in the operating theatre, where the pins are inserted using a pneumatic drill under fluoroscopic guidance. The next stop is the radiology department for calibration x-rays, after which the subject comes to the laboratory where the Fastrak system is mounted and the exercises are performed. The pins are finally removed by hand in the laboratory using a T-handle clamp.

The required mobility of the subject leads to a modular design of the sensor mounting system. Custom design fixation devices were machined to attach the Fastrak sensors to the subject's pins. Three generations of these Fastrak mounts have come into being since the first experiment, with each iteration improving upon its predecessor.

The need for custom mounts arises from the unique nature of the experiment. Design goals include: stable pin fixation; minimising the use of metal; reducing the size and the weight of the construction; simplifying the method for mounting and removing the holders; and making the design compatible with the calibration method.

The first parts to be used are the pin mounts which are attached to the pins in the operating room. When the subject arrives in radiology, calibration attachments are slid onto the mounts and two orthogonal radiographs are taken with them in place. From this point on, the pin mounts must remain fixed in their position since the radiographs will be used to calculate the relationship between sensors and vertebrae. In the exercise laboratory the calibration attachments are removed and the Fastrak attachments with a Fastrak sensor installed are fixed to the pin mounts.

The key premise of this technique is that the sensor, pin and vertebra remain a rigid unit throughout the experiment. Therefore, stable binding of pin and sensor via the holder is crucial, although in certain limited cases, a rotation of a mount can be corrected post-experimentally. Minimising the weight of the holder also serves as a means to reduce the potential for holder slippage as well as pin vibration. Since these holders protrude from the back of the subject, the size of the holders should be kept small to prevent possible collisions with each other or surrounding objects resulting in harm to the subject, or disturbance of the pin-holder configuration. The use of metal in the design must be kept to a minimum because eddy currents in conductive material disturb the magnetic fields created by the tracking system. Also, the mechanism for attaching the calibration and sensor parts to the pin mount must be precise, convenient and should not require any undue force or torque that may move the holder about the pin.

The first holder's construction was fabricated with Plexiglas® and a set-screw was used to clamp the pin in a receptacle in the holder. The mounting system consisted only of two parts, the pin mount with the sensor screwed to it, and the calibration attachment that slid into place along a grove in the mount. Not only was the design bulky and heavy, but it didn't bind to the pin as well as desired. In addition, the Plexiglas didn't withstand the sterilisation process of alcohol bathing and consequently suffered structural degradation over time.

A second design reduced the size and weight of the holder considerably but it still employed the set screw fixation mechanism and the Plexiglas material. Consequently, it too suffered from a less than perfect binding and material degradation.

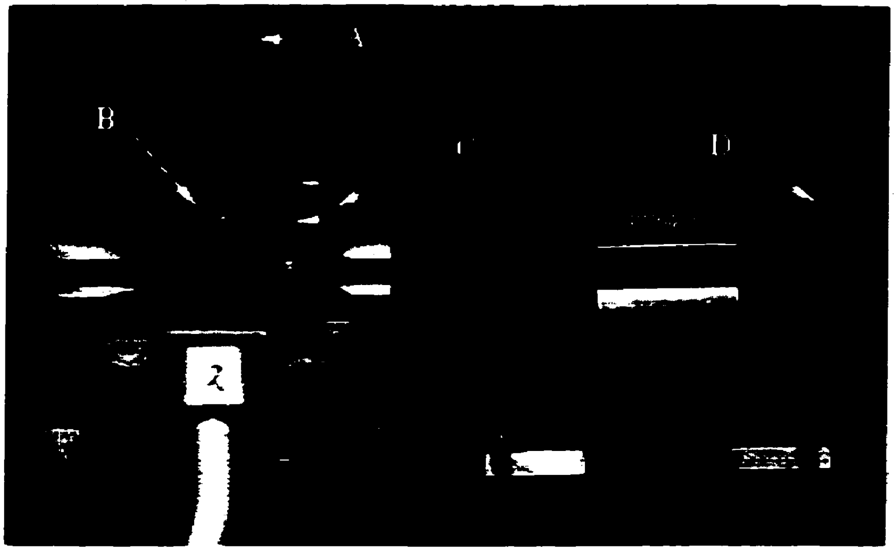

Figure 3-1 - Second Generation Pin-mounts: Shown on left, Fastrak sensor (2) attached to pin-mount. The mount is fixed to a pin (A) using a set-screw (B). On right, calibration attachment and metal bearings (D) which slides into grove of pin-mount (C).

The third and current generation was radically redesigned. Spurred by the need to instrument three vertebrae, the current model mounts to the pin in a staggered, lateral geometry that provides more space between pin-mounts. Since this new geometry results in a lever arm that increases the chance of rotation about he pin, a better pin fixation mechanism was designed. A threaded stainless steel wedge is guided by the slanted wall of a recess in the pin mount. This wall pushes the wedge against the pin as a set screw pulls the wedge further into the recess. The screw faces posteriorly and is easily accessible. The mechanical advantage of the wedge and its curved pin-contact surface results in a sound binding that is far superior to the previous designs.

Figure 3-2 - Third Generation Pin-mounts: Three pin-mounts fixed to the subject's pins in a staggered lateral configuration. A calibration attachment is shown in the surgeon's hand, ready to slide onto a pin-mount.

The calibration and the sensor attachments smoothly slide over the pin mount and are fixed in place with three turns of another set screw. Copolymerisat or POM-C material was used for the pin mount and attachments. POM-C is less brittle, lighter, easier to machine, and more amenable to the sterilisation process than Plexiglas.

The Fastrak field emitter, to which the positions of the sensors are referred, was originally placed on a jig near the subject during the exercises. This set-up was cumbersome, and during certain exercises, like flexion/extension ranging, the distance from source to sensor became too great and there was considerable distortion in the measurements. It was determined that a distance of 20 to 40 cm separating sensors and source provides optimal measurements. Therefore the solution was to modify a backpack and use the frame as a harness to be carried on the subject's upper back for the course of the experiment.

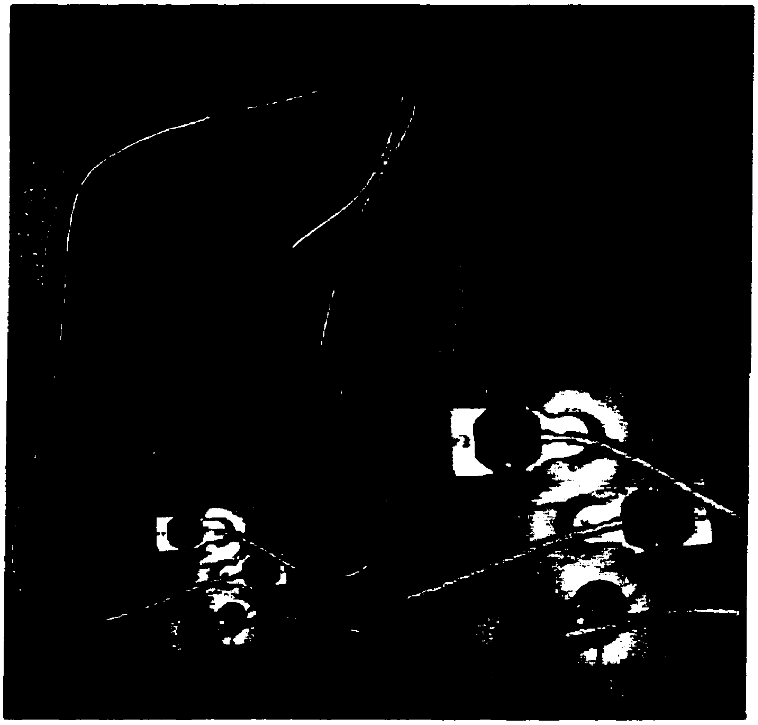

Figure 3-3 - Subject Wearing Experimental Montage: Shown are the three Fastrak sensors attached to the subject's pins by the third generation pin-mounts. The transmitter is the black cube in the centre of the harness.

This approach keeps the receivers within optimal distance of the source, but the subject's orientation relative to the world is not known unless an unused sensor is fixed to a jig resting on the floor. It was decided that the loss of world orientation was acceptable considering the gain in segmental motion accuracy when the transmitter is worn on the subject's back.

3.2.2 Data Acquisition Hardware and Interfacing

The data acquisition system is centred on two Macintosh Quadra 650 computers with one having a GPIB interface, and the other a digital and analog I/O board. The computers are connected and synchronised by an Ethernet (TCP/IP) connection, and the computer controlling the Fastrak data acquisition controls the computer acquiring analog data. The sensor hardware includes the Fastrak system, strain gauges, foot strike sensors and the analog signal conditioners. For most experiments, only the Fastrak system, foot strike sensors and signal conditioners are used while the other hardware was employed for validation purposes on a limited number of subjects.

3.2.2.1 Strain Gauges

To study the degree of pin bending during the experiments, which is an obvious potential for error, special pins augmented with strain gauges were fabricated by an in-house technician.

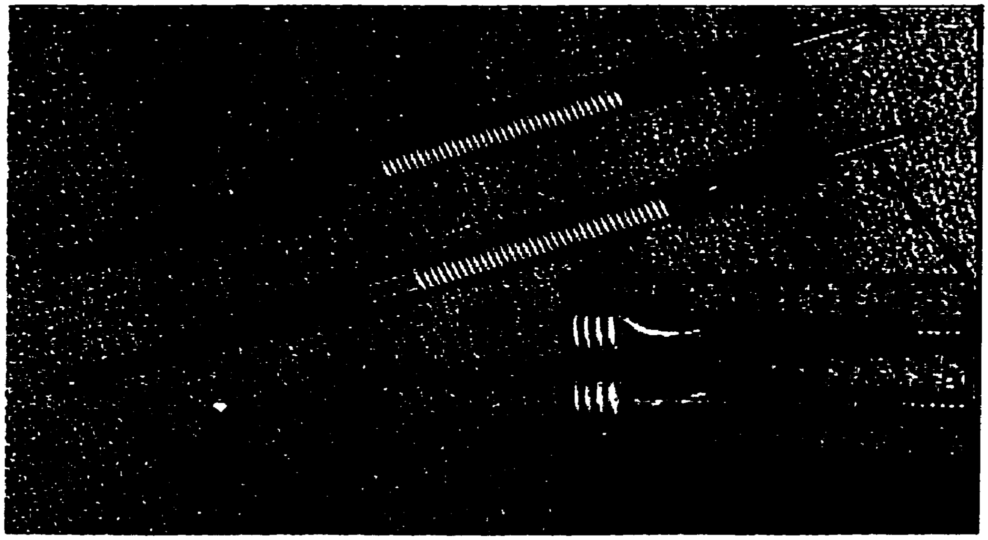

Figure 3-4 - Strain Gauge Augmented Pins: Two strain gauge augmented pins ready for insertion.

Pairs of semiconductor strain gauges (ESB-160-1000, Entran Devices Inc., Fairfield, NJ) were bonded along the pin's axis 20.5 mm to 25.5 mm from the tip. Teflon insulated wire attaches the semiconductors to an external bridge circuit. To protect the instrumentation from the sterilisation and pin insertion processes, silicon tubing was bonded over the pin and strain gauges. A laser inscription on the pin defines the orientation of measurement of the pin's deformation and is used as a reference by the surgeon during insertion. The strain gauges are connected to half-bridge circuits with a 3.0 V excitation voltages and the analog output signal is low-pass filtered at 20 Hz and amplified by a gain of 33 prior to being sampled at 200 Hz.

3.2.2.2 Foot Sensors

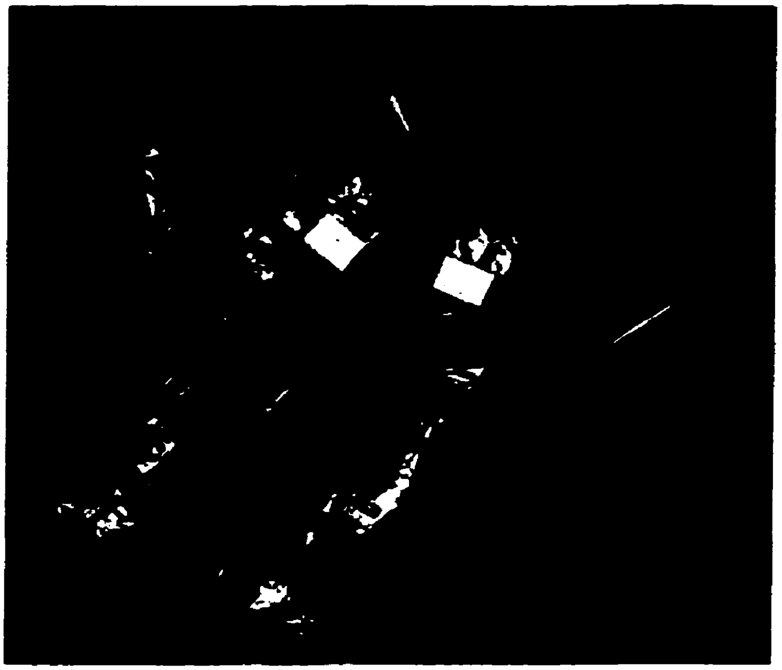

Figure 3-5 - Foot sensors for gait correlation

In order for us to study gait, the heel and toe strikes of both of the subject's feet must be correlated with the kinematic data. Shoe inserts with pressure sensitive resistive devices in the heel and toe are used to convert the gait events into electrical signals. The data acquisition circuit for each channel consists of an excitation source (10 volts), a voltage divider circuit comprising the resistive sensor element, a signal conditioner, and an A/D converter. The low-pass signal conditioners, each with unity gain and 100 Hz cut-off frequency, filter the voltage across the sensors and provide the excitation voltage as well. The filtered signals are sampled at 250 Hz with the Macintosh using the analog input channels of a National Instruments multi-input/output board (NB-MIO-16H).

3.2.2.3 Fastrak

As described in chapter 2, the Fastrak system consists of one transmitter, up to four receivers and a systems electronics unit (SEU). The SEU drives the transmitter which creates a low-frequency magnetic near field within which the receivers sense their position. The signals from the receivers are sampled by the SEU which uses an algorithm to compute each receiver's position and orientation relative to the transmitter. The SEU sampling frequency is 120 Hz which is multiplexed for each receiver. This project used two or three receivers with a resulting sampling frequency of 60 Hz or 40 Hz respectively.

The receivers are light and small enough to be mounted on the pins and not perturb the kinematics. Each receiver weighs 270 grams and is 5.3 cm wide and long and 5.8 cm tall.

The Fastrak is interfaced to the Macintosh computer using GPIB communication protocol (IEEE 488.1 standard) rather than the optional serial interface. This requires an NB-GPIB-488 interface board for the Mac (National Instruments).

3.2.3 Software Design

Software to control the experiment, data acquisition and post-processing was developed within the LabView (National Instruments) software environment. LabView has extensive libraries and drivers for data acquisition and eliminates the need for a programmer to write low level code for graphical user interfaces and device drivers. The language itself is similar to C and incorporates many of its constructs but does so in a graphical rather than textual form.

The Fastrak system is controlled via the GPIB interface with its own language of ASCII commands. A subroutine in LabView was written to handle all incoming and outgoing messages to the Fastrak, and a library of all the Fastrak commands was built upon this subroutine. The controlling software for the experiment, known as the '*in-vivo* control software', uses this library to initialise and retrieve data from the Fastrak system.

3.2.3.1 Graphical User Interface Design

The user interface for the *in-vivo* control panel is designed to be as simple as possible while maintaining the full functionality and flexibility necessary to run the experiment. The screen space is logically divided according to task. System initialisation controls are located at the top of the screen and disappear once the system is initialised, while the centre of the screen has text input boxes, buttons and menus to control experiment settings and input data specific to the test subject. In order to promote exercise consistency from one subject to the next, every exercise is listed in a pull-down menu and once selected, the description of the exercise is shown. Any divergence from the description can be typed into the 'comment' window by the observer.

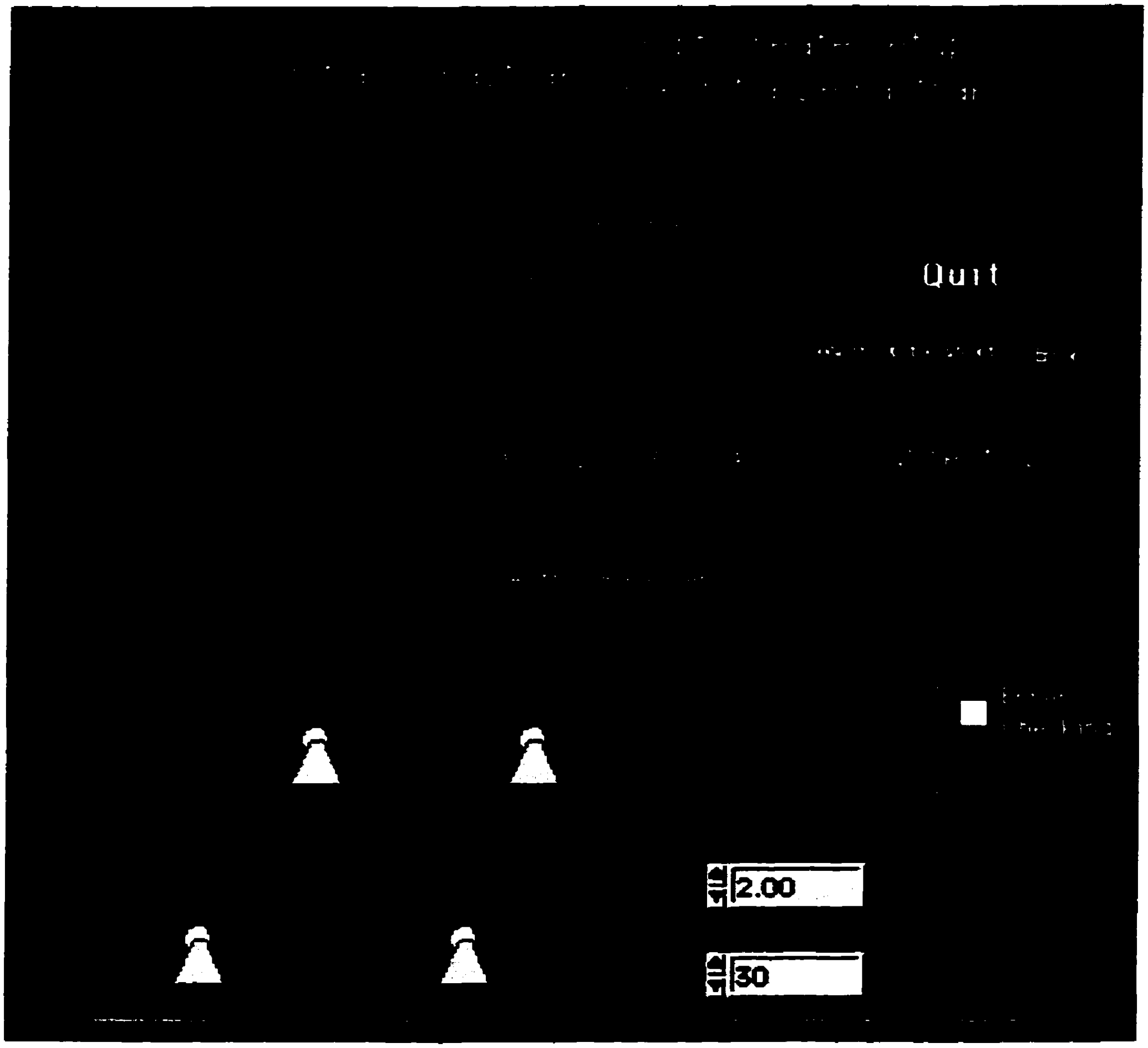

Figure 3-6 - *In-vivo* Main User Interface

All the controls for analog data acquisition are grouped together on the user interface near the bottom of the screen, with selector switches to turn the analog acquisition on or off, and select whether the acquisition will be done on the local computer or by a remote slave. The controls for external triggering by an active high or low signal are located at the very bottom of the screen, which allows the data acquisition process to be linked to an external event such as fluoroscopy acquisition.

At the end of the exercise, when the operator presses 'End', a dialog box is presented showing the same exercise selection menu and comment text box for confirmation and possible editing before the record is saved to disk.

3.2.3.2 Initialisation Procedure

There are many configurable settings and features for the Fastrak, analog input and digital output systems. An initialisation program was created to facilitate the configuration procedure that includes a graphical user interface to alter settings and save configuration files to disk. This program is accessible from the *in-vivo* control panel but normally the user simply loads a pre-saved settings file that automatically configures the system.

3.2.3.3 Acquisition Sequence

Once the user presses the 'Begin' button, the program enters an acquisition loop until the 'End' button is activated. Prior to the acquisition loop, a sequence of events execute based on user-selected options. First, the active receiver list is sent to the Fastrak controller which activates the desired receivers. If external triggering is activated, the sequence does not continue until the expected signal is received on the designated analog port or a timer reaches a time-out value. If analog data acquisition is on and a remote computer is being used, a signal is then sent over the Ethernet connection to the slave computer to start analog acquisition and the sequence waits for start confirmation before continuing. In order to synchronise a video camera, as well as inform the subject and researchers that acquisition has begun, a signal is then sent via the computer's serial port to a relay, which causes a lamp to flash.

The program now enters a poll and retrieve loop that continues until the user presses the 'End' button. The lack of data buffering requires the process to be streamlined as much as possible to keep up with the flow of Fastrak data. Since the number of samples is not known a-priori, the first coding of this loop used dynamic memory allocation, but it was found to be too slow due to LabView's poor memory management. It is not possible to change LabView's memory subroutines, therefore an alternate loop scheme was devised. Now, memory for an array large enough to store the longest record is allocated prior to the acquisition loop (about 120 seconds worth of data) and an error indicator lights-up on the *in-vivo* control panel if the acquisition exceeds the array limits. After the final loop iteration, the array is truncated to the number of valid entries to save data storage space. If analog acquisition was active during the loop, a signal to stop it is sent. The data are passed to a subroutine which checks each record for an error message from the Fastrak. If an error is detected, a error light is activated on the control panel and a dialog window is presented to the user.

The data are then passed to the storage subroutine which presents a confirmation dialog to the user. At this point, the user has the option to store or discard the data, and edit comments. If the user elects to keep the data, they are appended to the subject's data file in binary format.

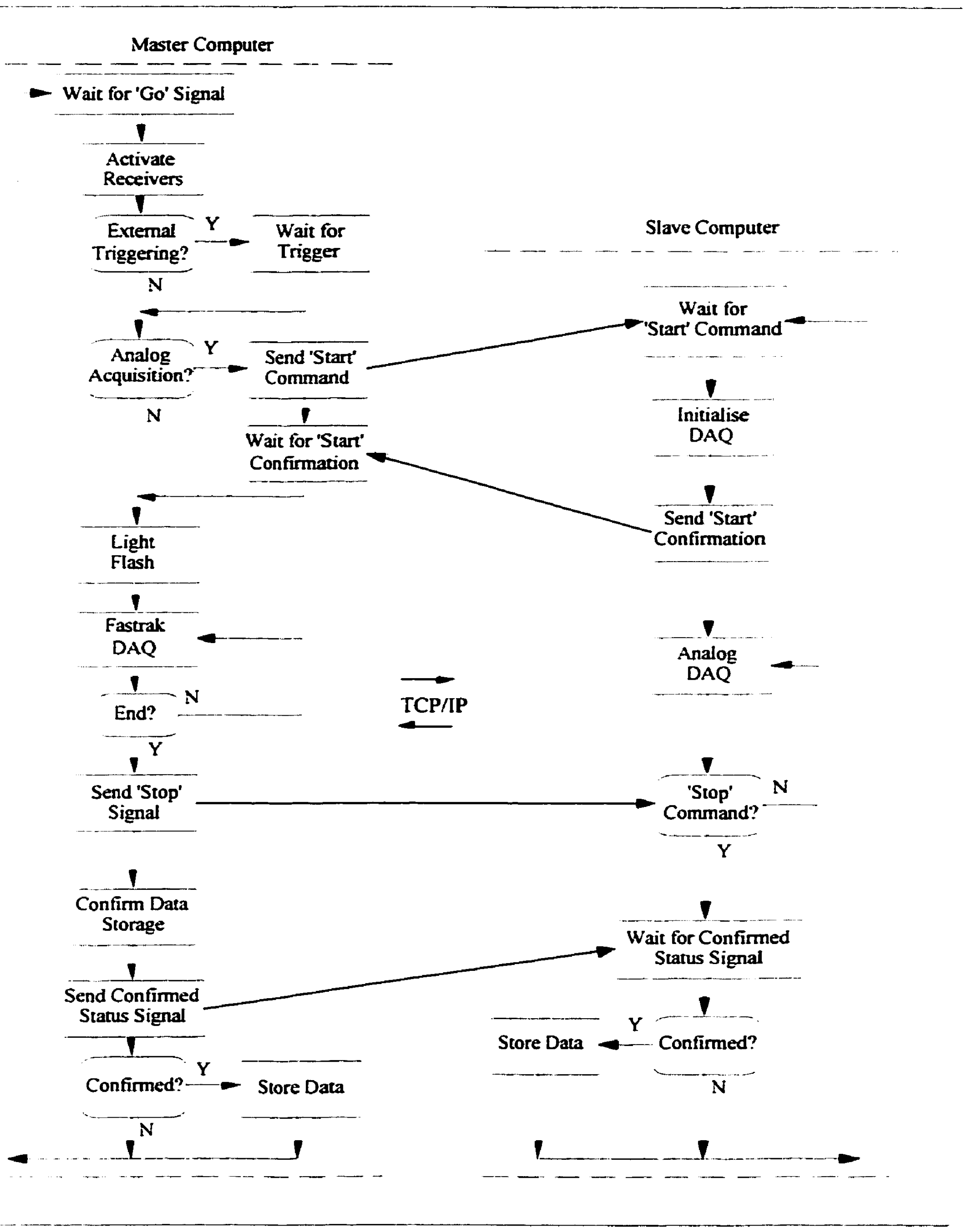

Figure 3-7 - Acquisition Sequence Flow Chart: The user interacts only with the master computer and it sends signals to the slave via TCP/IP.

3.2.3.4 Data Storage

A record of data consists of a two dimensional array of strings of position data, a time stamp and a record description string. No further processing is performed on the data due to the limitation in processing power of the Mac, which was kept busy polling and reading from the GPIB port. At the end of each exercise the samples from the Fastrak are saved in binary format to a file on the hard disk.

3.3 Calibration

The kinematics measured with the Fastrak sensors describe the motion of the sensors themselves rather than the motion of the vertebral bodies of interest. However, there is a relationship between the sensor's motion and that of the vertebral body to which it is attached. The relationship, known as a co-ordinate system transformation (CST), is defined by the physical connection of sensor, holder, pin and vertebral body, and is established via a calibration procedure prior to data acquisition. The CST describes, in mathematical terms, how to convert the position and orientation of one co-ordinate system to that of another. In this case, the conversion is from sensor to the vertebra's superior-endplate. Since internal anatomical distances are required, bi-planar x-rays (lateral and antero/posterior projections) are used to image the lumbar region with the pins and calibration mounts in place. From these radiographs, the CST's for each sensor-vertebral body pair are calculated.

3.3.1 Calibration Attachment

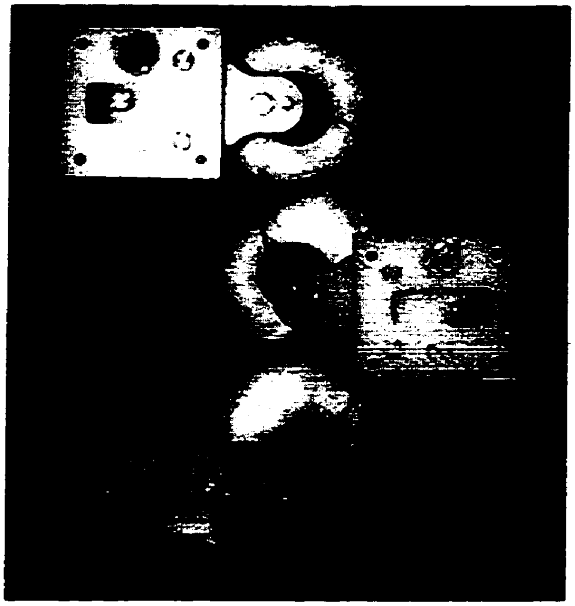

Figure 3-8 - Calibration Attachments

A small calibration attachment (40mm x 40mm x 5mm), with four small metal bearings embedded in each corner, slides onto the mount which binds to the pin. The body of the attachment is radio-translucent so only the bearings are visible on the x-rays along with the pin and anatomy. The calibration x-ray must image both the calibration attachment and the spine, but because part of the film is subject to direct radiation with no tissue absorption, a tissue compensator was used to partially cover the film. This increases the image contrast between the bearings and their surroundings by bringing the x-ray exposure into the linear range of the film. Even so, the bearings are difficult to see unless a strong lamp is used to back-light the film.

3.3.2 Computer Assisted X-Ray Analysis

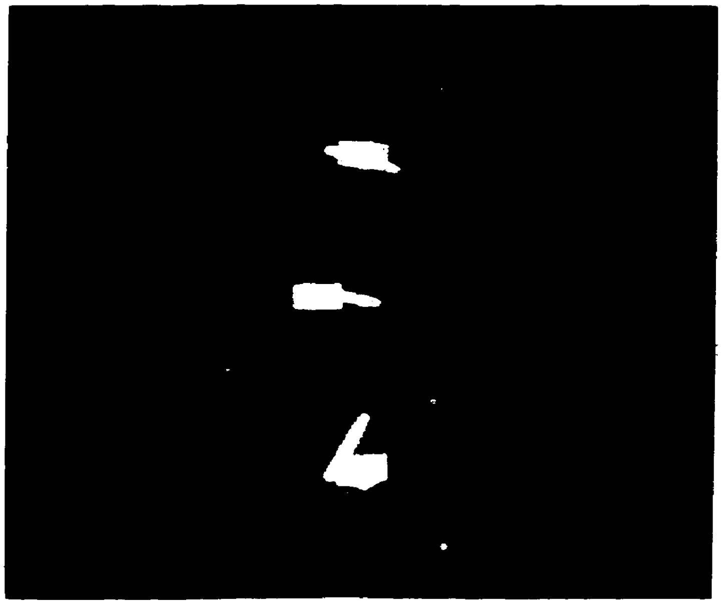

Figure 3-9 - A/P Radiograph

The process of measuring distances on the x-rays with a ruler and then calculating the CST is tedious and error prone. To relieve the researchers of this task, an X-Ray digitising method was developed. Using a light-box, key landmarks are marked on the film and digitised with a digitizing tablet. The series of x, y co-ordinates are stored in an ASCII file and read by a program written in LabView. The software calculates the CSTs and passes the results to the post-processing subroutine.

Figure 3-10 - Lateral Radiograph

3.3.3 X-Ray Measurements And CST Calculation

Sixteen points from the two orthogonal x-rays are used to determine the CST of a sensor to it's corresponding vertebral body (see Figures 3-11 and 3-12). To completely describe the transformation from the sensor to the vertebral body's superior-endplate, three linear offsets (x, y, z) and three angular offsets (a, e, r) with respect to the sensor's reference frame are required.

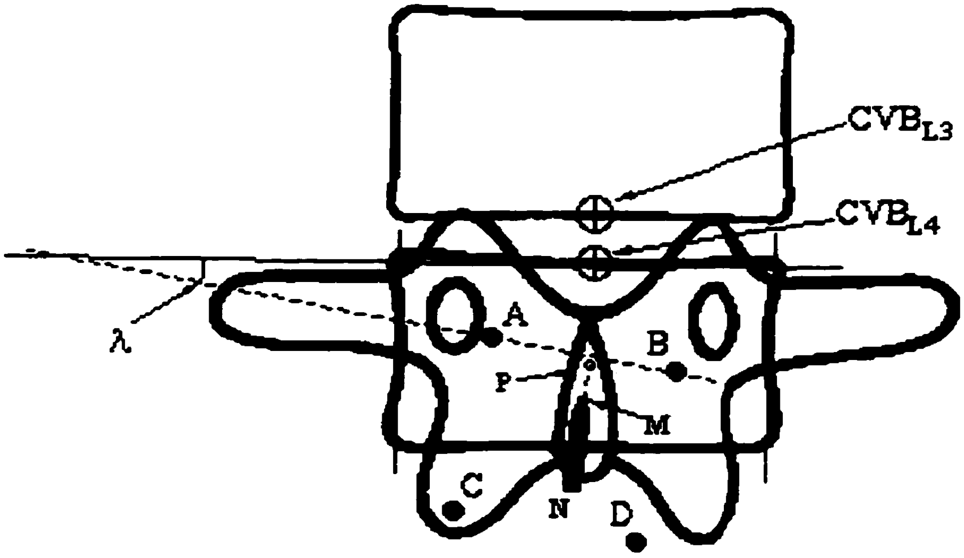

Figure 3-11 - A/P Radiograph Schematic Showing Landmarks

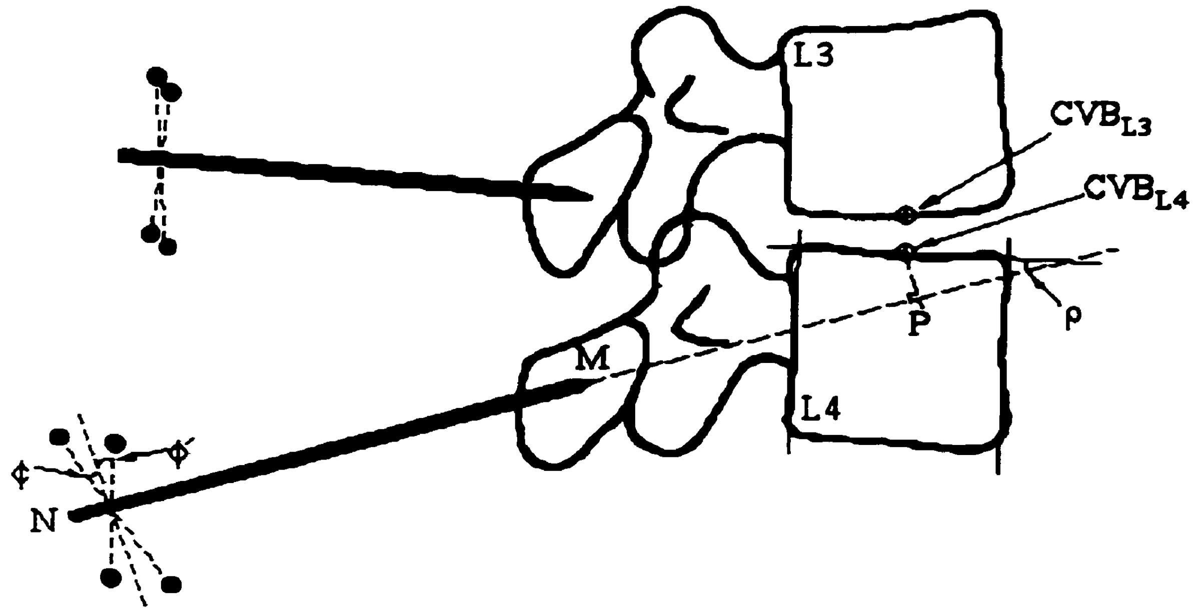

Figure 3-12 - Lateral Radiograph Schematic Showing Landmarks

Referring to the labels in Figures 3-11 and 3-12, the calculation of the six parameters are as follows:

3.3.3.1 Linear Offsets

z is defined as the distance from the electrical centre of the sensor to the CS of the endplate's centre along the sensor's z axis.

$$z = \frac{\overline{\mathrm{PN}}}{\mathrm{Mag}_{\mathrm{pn}} \cos\theta} + Z_{off} \qquad \text{Equation 3-1}$$

where θ is the angle that the pin makes with respect to the plane of the radiograph and can be found from the two angles ϕ and ϕ' formed by the steel ball markers. The relationship between θ , ϕ and ϕ' is:

$$\theta = \cos^{-1}\left(\sqrt{\tan(\phi)\tan(\phi')}\right) - \frac{\pi}{2} \qquad \text{Equation 3-2}$$

$\mathrm{Mag}_{\mathrm{pn}}$ is a term used to correct for the magnification in the lateral radiograph and is dependent on the depth of an object in the radiographic field. Its value is determined by comparing the actual pin length with that measured on the radiograph with accommodation for the angle θ. Z_{off} is the distance from the sensor-end of the pin to the electrical centre of the sensor along the sensor's z axis.

Using the A/P radiograph, a vector starting at the sensor end of the pin and ending at the pin's tip is multiplied by a constant which scales the vector to reflect the distance n-m on the lateral radiograph. The projected tip's x, and y offsets to the centre of the vertebral body's endplate ($x_{projected}$, $y_{projected}$) are used to calculate the real distance from the electrical centre of the sensor to the CS of L4 with

$$x = \frac{x_{projected}}{\mathrm{Mag}_{\mathrm{cvb}}} + X_{off} \qquad \text{Equation 3-3}$$

$$y = \frac{y_{projected}}{\mathrm{Mag}_{\mathrm{cvb}}} + Y_{off} \qquad \text{Equation 3-4}$$

where $\mathrm{Mag}_{\mathrm{cvb}}$ is a term used to compensate for the radiographic magnification in the A/P radiograph at the depth of the projected tip. An initial estimate of the magnification is obtained by comparing the distance between bearings on the X-Ray with the actual value. Since $\mathrm{Mag}_{\mathrm{cvb}}$ is at a different depth in the radiographic field than the calibration attachment, the initial magnification estimate is modified by compensating for this change in field depth using similar triangle ratios. X_{off} and Y_{off} are the distances from the sensor-end of the pin to the sensor's electrical centre along the sensor's x and y axes respectively.

3.3.3.2 Angular Offsets

The angular displacements for a, and r are measured directly from the radiographs as the angles λ and ρ respectively. The angle the sensor is rotated about its y axis relative to the CS of L4 is chosen to be zero. The difficulty in using landmarks for determining the orientation of the endplate along this axis justifies using the assumption that the pin lies in the sagittal plane.

3.3.3.3 Sensor/Endplate CST

With the six parameters calculated, the CST from sensor to endplate can be expressed as the following 4x4 matrix

$$CST(x,y,z,a,e,r)=\begin{bmatrix} \cos a\cos e & \cos a\sin e\sin r-\sin a\cos r & \cos a\sin e\cos r+\sin a\sin r & x \\ \sin a\cos e & \sin a\sin e\sin r+\cos a\cos r & \sin a\sin e\cos r-\cos a\cos r & y \\ -\sin e & \cos e\sin r & \cos e\cos r & z \\ 0 & 0 & 0 & 1 \end{bmatrix}$$

Equation 3-5

In the above expression, x, y, and z are the three linear offsets and a, e, and r are the three Euler angle displacements -- azimuth, elevation and roll respectively. The Euler angles define a strict rotation sequence: first about the z axis, then about the y axis and then about the x axis of the sensor's co-ordinate system.

Given two co-ordinate systems, C1 and C2, described with respect to the reference co-ordinate system a CST, T, can be found which describes C1 with respect to C2. T can be calculated by the matrix multiplication

$$[T] = [C2]^{-1}[C1]$$ Equation 3-6

where $C2^{-1}$ is the matrix inverse of C2 and represents the CST of the reference system to C2 *with respect to C2.* By pre-multiplying both sides of equation (1.2) by C2, C1 can be expressed as

$$[C1] = [C2][T]$$ Equation 3-7

which is useful in our case where T is the constant CST of L4 to its sensor, $[L4 \rightarrow R2]$, and C2 is the variable CST of the receiver to the reference system (output from the Fastrak system), $[R2 \rightarrow Ref]$. The resulting matrix C1 is the CST of L4 to the reference system, $[L4 \rightarrow \mathrm{Ref}]$. Rewritten with more meaningful terms, equation (1.3) becomes

$$[L4 \rightarrow \mathrm{Ref}] = [R2 \rightarrow \mathrm{Ref}][L4 \rightarrow R2] \qquad \text{Equation 3-8}$$

Similarly, L3 relative to the reference system is calculated from

$$[L3 \rightarrow \mathrm{Ref}] = [R1 \rightarrow \mathrm{Ref}][L3 \rightarrow R1] \qquad \text{Equation 3-9}$$

Since we are interested in relative movements between L3 and L4, the following matrix multiplication finally allows the data to reflect this relative motion

$$[L3 \rightarrow L4] = [L4 \rightarrow \mathrm{Ref}]^{-1}[L3 \rightarrow \mathrm{Ref}] \qquad \text{Equation 3-10}$$

As a short form for the above notation for CSTs, instead of $[L4 \rightarrow R2]$, the same CST matrix may be written as ${}^{R2}L4$ which is read, “L4 with respect to R2 in R2’s CS.”

3.4 Data Post-Processing

After the experiment, the data are in a raw state and need to be converted into useful information via a concatenation of mathematical operations. Each sample in time records the co-ordinate system of each Fastrak sensor. The conversion is performed off-line and currently takes about 90 minutes per experiment. The CSTs derived from the calibration are used to transform the data to reflect relative segmental motion. A non-linear median filter is used to smooth the data. This first order non-linear filter replaces the current point with the median of the current point, previous point, and the following point. The filter will smooth a one point 'glitch' while preserving edge sharpness, thus providing characteristics of both high-pass and low-pass filters. The glitch-free relative segmental motion was then filtered forward and backward through a second order Butterworth filter (cut-off frequency = 5.4 Hz) resulting in a fourth-order Butterworth filter with no phase shift.

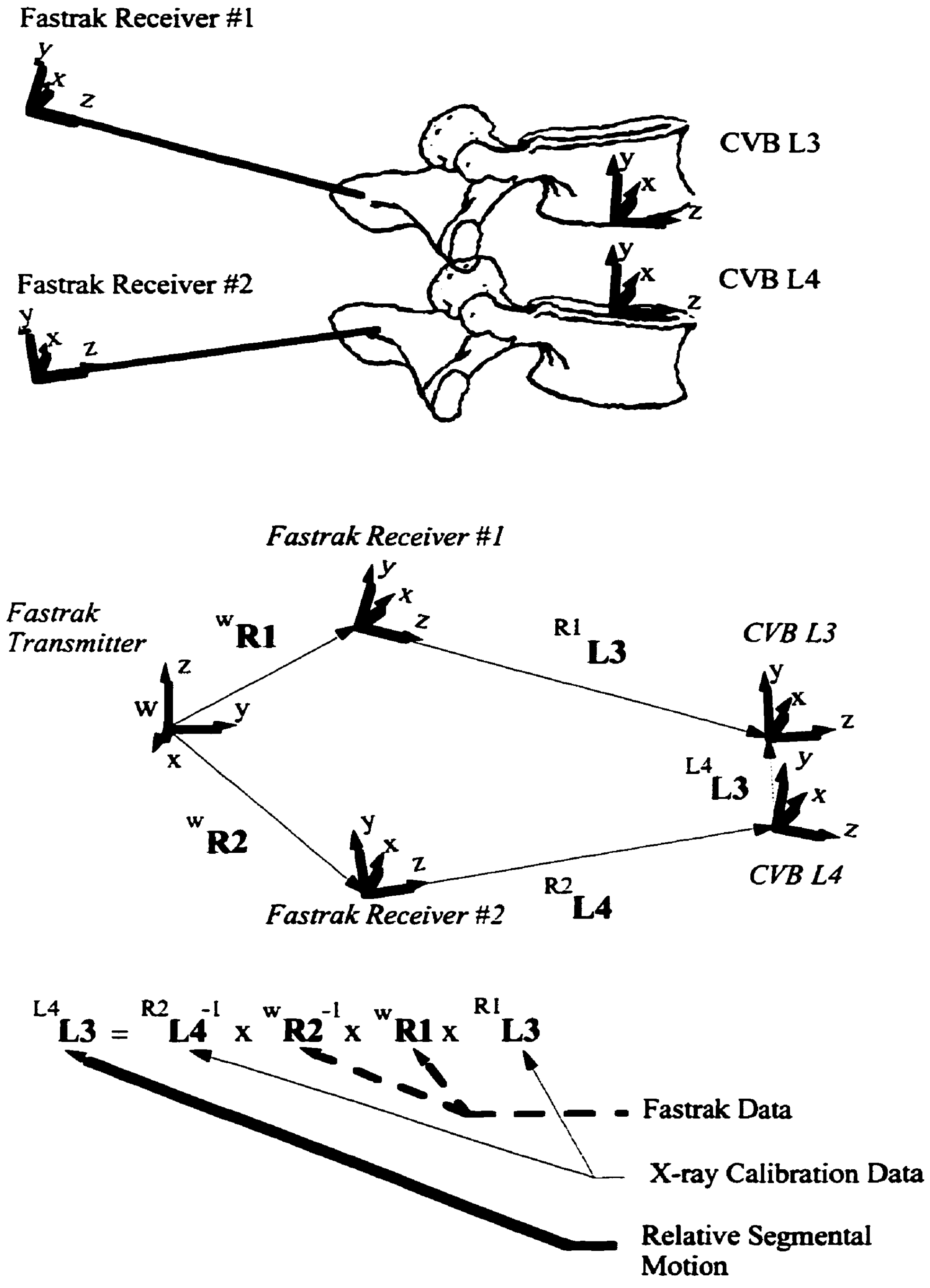

Figure 3-13 - Relative Segmental Motion CSTs: The equation at the bottom of the figure is evaluated during post-processing for each kinematic sample instance.

3.5 Validation Method

The method was validated by a series of experiments which assessed the accuracy and reliability of the tracking system. The dynamic accuracy of the kinematic measurement system was quantified by having subjects perform the exercises while wearing the full experimental montage with the addition of a wood block, belted around their waist, with two sensor-mounted pins drilled into it. The placement of the receivers relative to each other, the transmitter, and the subject were similar to those in the experiments and realistic CSTs were used to transform the data. The transformed data then represents the relative position between two virtual segments. Since the receivers are firmly fixed to the block, they should have an invariant spatial relationship, and any displacement observed in this virtual segment represents the system's measurement error.

3.5.1 System Reliability

In order to study dynamic pin deformation, a pilot study with four subject's was conducted. The standard Kirschner wire's were augmented with semiconductor strain gauges and measurements were recorded with them throughout the standard exercises via the analog input channels. All four subjects had instrumented pins inserted into the L3 vertebra and one had an additional instrumented pin in L4. Two factors suggest that deformation would be greatest in the cranio-caudal direction: 1) the skin shift would be largest in this direction, especially for flexion/extension exercises, and 2) the quasi-strict vertical orientation of the muscles and ligaments in this region would exert force in this direction. The upper pin was expected to be subject to the most amount of skin traction because skin shift increases in the cranial direction.

Instrumented pins were inserted into a wooden block to calibrate the strain gauges to a depth equal to the intra-operative insertion depth measured from the lateral radiographs. A micrometer displaced the pin laterally by pushing on the pin at a fixed height in the plane of the strain gauge pair, which produced a signal voltage proportional to the average strain along the length of the semiconductor (5 cm). The pin's bending radius was estimated at the centre of the measuring surface. To estimate the error due to pin deformation, the signal measured during the experiment was compared with the post-experimental calibration (see Appendix).

Since the force distribution along the bone-skin distance of the pin *in-vivo* is unknown, two force distribution models were used to calculate the pin's deformation from the signal voltage. One beam bending model assumes a uniform force along the bone-skin length, while the other assumes a point force is applied at the level of the skin (see Appendix). Both models were used to estimate the error resulting from pin deformation.

4. MRI Acquisition

Three dimensional animation of spinal kinematics requires 3-D information of the bony surface of each vertebra. Magnetic resonance imaging was selected as a non-invasive and non-ionising method to obtain this information. Unfortunately, there are difficulties with MR imaging of the lumbar spine due to motion artefacts caused by the surrounding vasculature and due to the region of interest's depth within the body. At least seven parameters may be adjusted over a continuous range of values to maximise image quality, resulting in a very complex and difficult decision on the choice of acquisition protocol. With the aid of a radiology technician, a number of potential protocols were chosen and a test subject underwent imaging with each. The 'perfect' image would have excellent contrast between the cortical shell of the vertebrae and the surrounding tissue, good resolution and a low signal-to-noise ratio. These being competing goals, the protocol selected was considered the best compromise while slightly favouring image contrast.

A fast 3-D gradient echo acquisition with TR=17.2 ms, TE=0.6 ms, and a flip angle of 40 degrees was used to image each subsequent subject on a GE Signa MR scanner. The image volume consisted of sixty slices spaced 2 mm apart along the antero-posterior direction with each slice having 256 x 256 samples (0.9375 mm uniform spacing) in the coronal plane. A surface coil, placed under the subject's back, was used to increase the signal to noise ratio.

The resulting images are still noisy -- with the noise increasing in the anterior and caudal directions -- but they have sufficient contrast such that the interface between the cortical shell and surrounding tissue is visible. In the images, the cortical bone appears dark because of its low water or fat content, the spongy bone in the interior of the vertebra is slightly brighter and the cerebral spinal fluid (CSF) is bright along with the ligamentous tissue and intervertebral disk.

4.1 Data Transfer And Conversion

All the subjects were scanned at the Montreal Children's Hospital (MCH) with a General Electric MR Signa 5 scanner. The sequences are stored on 4mm digital audio tape for transport because the scanner at the MCH is not accessible via the Internet or any network connecting the RVH and the MCH. The data are originally stored in GE's Signa 5X proprietary format which is structured with a fixed size control header, a variable header containing patient, acquisition and compression information and followed by the image data.

In order for the data to be imported and manipulated in AVS, a data input subroutine or module had to be written in C. Rather than start from scratch and write a program to first read the DAT tape -- which also is formatted using GE's proprietary format -- and then translate the data into AVS format, a Perl script available at the Brain Imaging Centre (BIC) at the Montreal Neurological Institute (MNI) already existed to read a GE tape and store the files on the hard drive in the MNI's Medical Image Net-CDF (MINC) data format. Then the BIC's Volume IO library, built on top of the Net-CDF library of image manipulation routines, provided functions to readily access header and image information. An AVS module, read_minc, was written in C that linked with Volume IO, Net CDF and AVS libraries.

Now, getting the data into the AVS environment is a simple two step process. First the data are sequentially transferred from DAT tape to the hard disk and optionally compressed, then the read_minc AVS module automatically reads the normal or compressed MINC image file and repackages the data in memory into a format that AVS understands.

5. Kinematics Visualization System

5.1 2D Visualization And Quantitative Analysis Software

Software was developed in LabView to analyse and display the results of the *in-vivo* experiments. All the analysis modules are accessible from a single graphical interface and all the tools were developed to be simple and to minimise the amount of user interaction since the task of analysing each exercise for each subject is tedious as is. All the analysis modules provided 2-D graphical displays of the results as well as tab-delimited ASCII tables which are easily imported into other software applications.

5.1.1 Software Functionality -- Overview

In addition to simply displaying 2-D graphs of the relative segmental motion and tabulating these results, other quantities need to be extracted from the data or the data need to undergo further processing.

Software tools were created to compile statistics for range of motion (ROM) quantities. An interactive 2-D graph was used to display the curves of one subject for a particular exercise and a local maximum/minimum detection algorithm computed the average ROM. Markers were overlaid on the graph to show the region of interest, and the calculated maximum and minimum for each cycle. The markers can be modified with the mouse if necessary, but usually no interaction was required. The results were stored and later passed to a statistical computation routine to provide values for the average, standard deviation, standard error and confidence intervals.

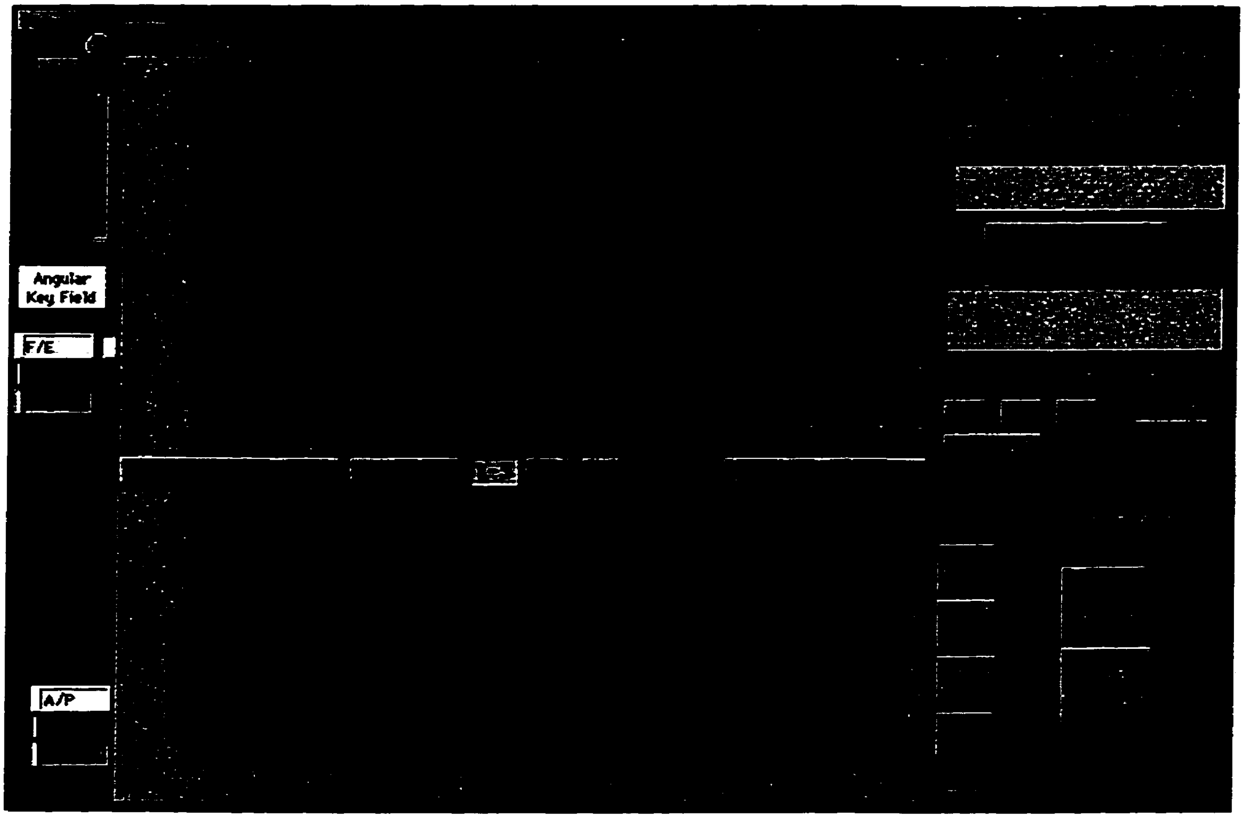

Figure 5-1 - Normalisation Analysis Module: Graphical user interface.

Since the standard deviations were large (even for the same exercise of the same subject), a normalising algorithm was added to normalise the motion over time. Each cycle of an exercise (which was repeated multiple times) was segmented and then normalised into 40 sample points. The amplitude of the motion was left unaffected. Each degree of freedom of a cycle from one subject was then averaged and a 2-D graph showed all the averaged curves for each subject for the given exercise. This facilitated pattern comparison.

The same data were needed for gait analysis, but the segmentation of the curves is governed by the gait events. A software tool automatically divided the curves into segments using the analog data from the foot sensors and then normalised, averaged and displayed the results.

5.2 3D MR Data Animation

Three dimensional computer animation provides the most intuitive and concise way of demonstrating the kinematics of a spinal segment. A number of processing steps are needed to convert the MR data into a usable form for animation. First the MR volume of voxels must be segmented into vertebral bodies, then a geometrical representation must be obtained by fitting a triangle-mesh to the vertebral body's surface. The geometrical surface representations for each vertebra are then sequentially manipulated with a stream of co-ordinate system transformations obtained from the kinematic measurements. The result is a time varying rendering of the relative motion of the vertebrae in 3-D.

5.2.1 Programming Environment

Advanced Visual System's software, AVS 5.3 (Waltham, MA) and a Silicon Graphics Indy (Mountain View, CA) was chosen as the development platform for the MR animation. AVS is a visualisation package with libraries for image processing, volume rendering and GUI development. The main advantages for using AVS is the large library of functions for image processing, 3-D rendering, animation and graphical user interface widgets.

5.2.2 Segmentation

The MR data are initially acquired as a block of image data, but for the purpose of animation, this block must somehow be divided or segmented into smaller, independent objects. The only information available to guide this segmentation is the voxel's intensity and location. The protons belonging to different tissues (e.g., bone, muscle, or fat) reside in dissimilar chemical environments and as a result, are distinguished by the intensity of their composite voxels. Therefore, adjacent voxels with similar intensities are considered to belong to the same tissue. It was this principle that was used to subdivide the volume into voxels belonging to different structures, namely the vertebral bodies made of cortical and spongy bone.

There are many algorithms available to segment image data [41-46]. The spectrum varies in the degree of human interaction needed for the process. Methods which require a large degree of human interaction are simple to program and as the input needed from a person is reduced, the algorithm complexity increases. At the simplest level, a user manually traces the contour of the vertebral body in each slice of the volume with no amount of computer intervention in the process. A computer may perform some image processing first by performing histogram equalisation or filtering to improve the quality of the image, but the selection of the boundary is still completely up to the user. Another method only requires the user to pick a 'seed' voxel and based on the seed's location and intensity a region growing algorithm could select an appropriate region of voxels to include in the vertebral body selection.

The MR images of the lumbar region were noisy, as mentioned in section 5 and as shown in the image on the right, and this severely limited the usefulness of computer aided boundary selection techniques. A region growing algorithm was developed in addition to a manual tracing tool and both are described below. In the end the manual tracing method was chosen for its simplicity and robustness since it relies on one of the most advanced pattern recognition systems: the human visual system.

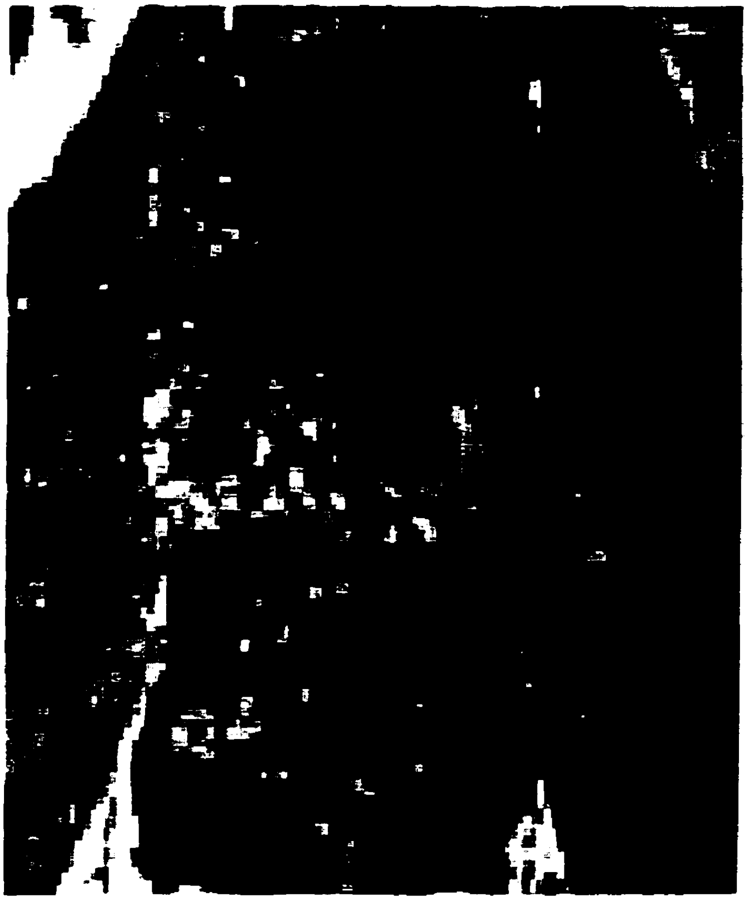

Figure 5-2 - Anterior MRI Slice of Lumbar Region

5.2.2.1 Region-Growing Algorithm

In an attempt to automate to the vertebral body selection process, a region-growing algorithm was coded in C and compiled as an AVS module. Using the intensity of the seed voxel, and the principal of connectivity, the algorithm grows a region around the seed, selecting all voxels that are considered to belong to the seed's region. This operation is performed recursively where the seed's neighbouring voxels are judged as belonging to the seed's region if their intensities are within a certain tolerance of the seed's intensity. Neighbours within tolerance are added to a list with the seed and their neighbours are then added to a FIFO queue and the algorithm reiterates selecting the next queue member as the seed. The algorithm terminates when the list is empty.

In theory, this should work well but in practice, the noise is a severe confounder and the large number of pixels that need processing make this method too slow and inaccurate to be practical.

5.2.2.2 Manual Tracing Tool

A manual tracing tool, which takes full advantage of human pattern recognition abilities and results in a simplified algorithm, was developed to segment the image volume. The user is able to select a two dimensional slice from the volume (coronal plane) and trace the contour of the vertebral body with the mouse. Facilities such as rubber banding, contour completion and an undo function were added to aid the tracing and make the program more user-friendly. Once the user indicates that the contour is satisfactory, the contour is copied to an empty volume of the same dimensions as the original. An algorithm then fills in the contour and sets all the voxel intensity values to 255. Once the contouring for each slice is complete, a corresponding 3-D solid object exists in the new, previously empty volume which is cropped to contain only enough volume to house the object.

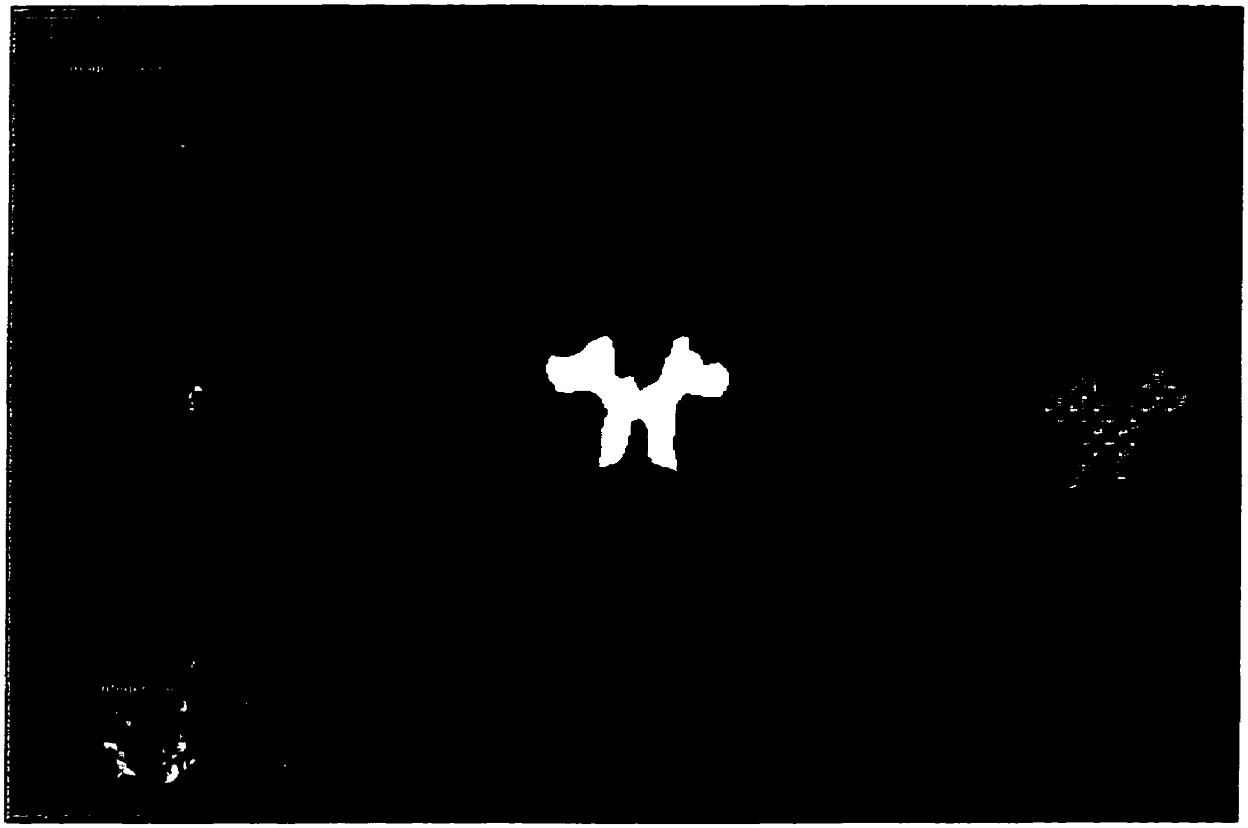

Figure 5-3 - Manual Tracing User Interface: The user traces the contours on each slice (left) and the corresponding filled region is shown (middle) and the current 3-D object (right).

5.2.2.3 Downsizing

To reduce memory requirements and processing time, the segmented volume is downsized using a tri-linear (3-D) sub-sampling algorithm. The trade-off is a reduction in surface detail or high spatial-frequency information with increased downsizing. The downsizing parameter is adjustable by the user. No problems with aliasing were observed during this step.

5.2.2.4 Iso-surface

The final step to obtaining an easily transformable object is to convert the voxel description to a geometry description. Most of the information in the voxel-map--namely, the inside of the objects--is not needed for an animation. Only the surface is required, so a considerable savings in memory is achieved by converting the volume to a mesh-geometry representation. Since the graphics hardware is optimised to render solids from a triangle mesh description, the iso-surface function was used to create such a mesh. The iso-surface module supplied with AVS takes an intensity value as a parameter and creates a mesh connecting all the voxels on the boundary of the input intensity. In this case, all the voxels belonging to the vertebral body are white (255) and the boundary voxels are black (0) so the iso-surface creates a geometry mesh of the surface. This is stored as an ordered list of triangle vertices, known as a poly-triangle mesh.

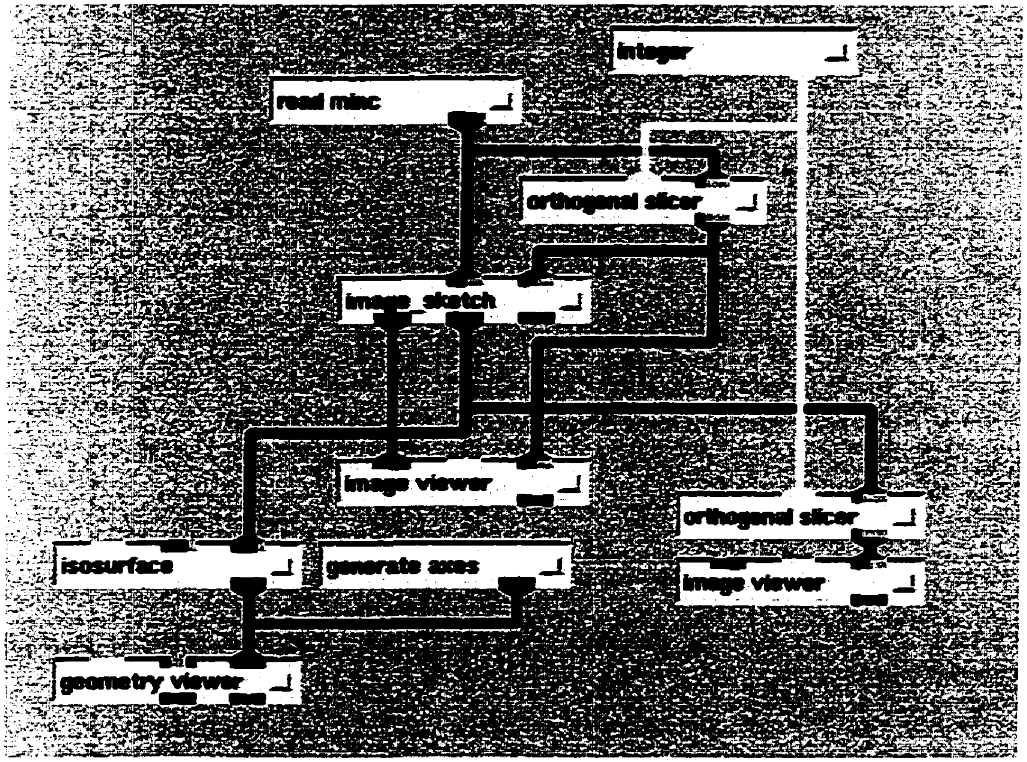

Figure 5-4 - AVS Network for Manual Tracing and Iso-surface Functions

5.2.3 Geometry Rendering

AVS5 has built-in capabilities to render geometry type objects as those created from the iso-surface module. Called the geometry viewer, AVS's interactive module supports many of the features for realistic 3D rendering. The user is able to display multiple geometric objects and control the position and orientation of the objects, the camera and the light sources. The geometry viewer can also be controlled by a script language, which is how the objects were animated for this project.

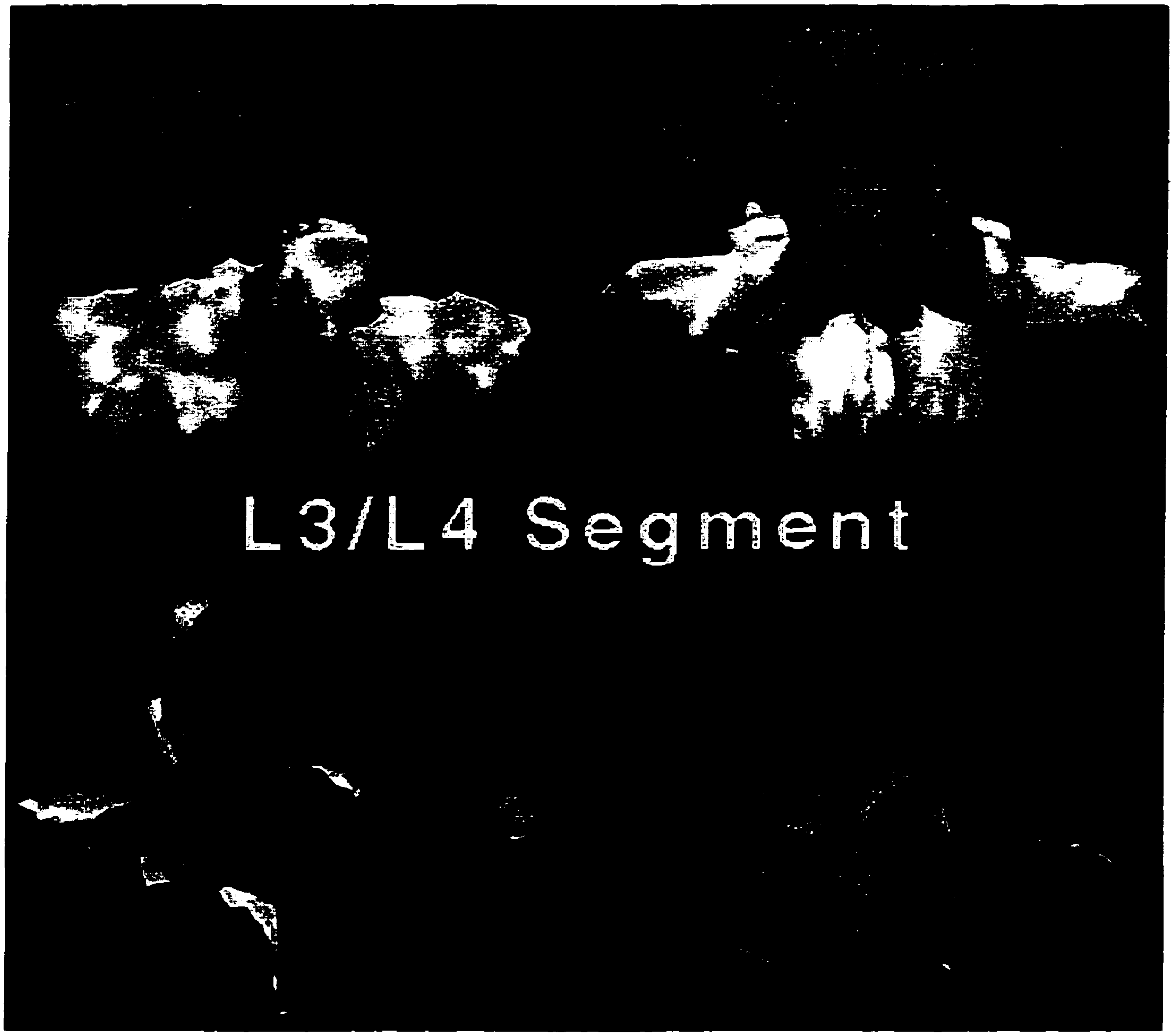

Figure 5-5 - Rendered L3/L4 Vertebral Segment

5.2.4 Animation

Now the data from the kinematic experiments are merged with the MR data to bring life to the geometrical objects created with the iso-surface module. The link is a script that is generated by a LabView program and interpreted by AVS's geometry viewer. The kinematic data describes relative motion between two vertebrae: motion of the centre of the inferior endplate of the superior vertebra relative to the centre of the superior endplate of the inferior vertebra. Therefore, the centre of rotation of the animation must be the same point on the superior vertebra. This is adjusted by simply measuring the centre of the proper endplate in 3D with a pointing tool in AVS, and using a script command to make that point the object's centre of rotation. The following lines are the first of a CST script which sets up the CS of the segment and then lists the object's new transformation matrices for the subsequent steps in time.

```
geom_set_center -obj 13 -14.420 37.320 15.000
geom_set_matrix -obj 13 -rx 0.147 -ry 0.028 -rz 0.437 -tx 0.012 -ty 0.007 -tz 0.005
geom_concat_matrix -obj 13 -rx 0.0388 -ry -0.0140 -rz -0.005 -tx 0.002 -ty -0.001 -tz -0.002
geom_concat_matrix  ...
```

If these steps are processed fast enough, they don't appear to be steps at all but rather a smooth animation describing the motion of the vertebral bodies.

6. Results

6.1 Validation of the Kinematic Data Acquisition System

The method's validity was evaluated by quantifying its accuracy and reliability. In the context of this system, accuracy refers to the expected error when measuring relative segmental displacements. It is mainly governed by the tracking system's limitations and the possible error amplification that may occur during the mathematical co-ordinate system transformations.

The issue of reliability--the system's objectivity in measuring true vertebral body motion--is also a concern and was systematically addressed. Reliability may be compromised by unstable pin fixation in the spinous process, a poor calibration, pin and/or bone deformation, and measurement distortion due to ferrous materials within the environment of the magnetic field.

6.1.1 System Accuracy

Accuracy specifications for the Fastrak receivers are provided by the manufacturer (Polhemus), but they apply to stationary measurements and can not be simply extrapolated and quoted as the accuracy values for segmental displacements. For this reason, extensive testing was needed to validate the system under experimental conditions. This includes the quantification of error due to the Fastrak system for *dynamic* conditions while using the co-ordinate system transformations (CSTs) to calculate relative segmental motion.

As described in section 3.5, the accuracy of the segmental measurements was assessed by having subjects perform the exercises while wearing the experimental montage plus a wooden block with the Fastrak receivers fixed to it. The receivers were therefore free to move in 3-D yet were constrained to have no relative motion. In the absence of any inaccuracy, the calculations to convert the sensors individual motion into a relative quantity should result in a static value throughout the exercise. However, a random distribution about a constant mean was observed that was not correlated with the subject's motion. Therefore a root mean squared (RMS) value was derived from a large series of sample points and used to quantify the error.

$$\text{RMS error}_i = \sqrt{(\bar{x} - x_i)^2}$$

This value encompasses the error due to the tracking system's inaccuracy; error amplification due to the CSTs; electromagnetic distortion due to metal in the environment; and error due to motion that is exceedingly dynamic with respect to the tracking system's sampling rate. The following tables (6-1 and 6-2) list the RMS error for segmental motion and a 95% confidence interval (CI) for each degree of freedom.

		RMS Error for Segmental Motion (degrees)	
Angular Motion	n	Mean	95% CI
Flexion/Extension	24	0.14	0.09 - 0.20
Lateral Bending	24	0.19	0.15 - 0.23
Axial Rotation	24	0.08	0.06 - 0.40

Table 6-1 - Dynamic RMS error for angular motion

Linear Motion	n	RMS Error for Segmental Motion (millimetres) Mean	95% CI
A/P Shear	24	0.20	0.16 - 0.25
Lateral Shear	24	0.38	0.29 - 0.48
Compression/ Distraction	24	0.32	0.25 - 0.40

Table 6-2 - Dynamic RMS error for linear motion

6.1.2 System Reliability

The method assumes that the receiver, Kirschner wire and vertebral body constitute one rigid body. Any deviation from this assumption, either as a permanent or transient position change in the vertebra-pin-receiver configuration, constitutes an error in the reported segmental motion.

As a test for a stable pin fixation in the vertebral body, a comparison was made between data measured with the subject in a neutral upright position before and after each experiment. Since there is difficulty in reproducing an exact posture for each comparative measurement, a pin's fixation was judged to be unstable only if there was an observed change greater than one degree in angulation or one millimetre in position in any of the three axes. Only two subjects' pins out of twenty-six were deemed unstable by this method, one of which had a single event of pin rotation that was corrected mathematically allowing the data to be included in the study population.

In addition to the pin fixation being unstable, a deformation of the pin itself is a potential violation of the rigid body assumption. As described in section 3.5, special pins augmented with strain gauges were used in four subjects to quantify the error in segmental motion measurements due to pin deformation. Calibration of the strain gauge pair revealed a highly linear relationship (R^2 = 0.999) between perpendicular displacement and signal voltage for all pins. Autoclaving did not alter the electrical characteristics either. The calculated errors from pin bending in the cranio-caudal direction (Table 6-3) were pooled for all full range-of-motion exercises and for all subjects. The mean relative segmental errors, estimated with beam-bending models, were 0.30 degrees (range 0.07 - 0.66 degrees) for angular displacement and 0.37 millimetres (range 0.09 - 0.83 millimetres) for linear displacements.

Type of Exercise	Subject	Angular Error (degrees)		Linear Error (millimetres)	
		Uniform*	Point*	Uniform	Point
Flexion/ Extension	1.	0.47	0.48	0.58	0.61
	2.	0.15	0.14	0.18	0.17
	3.	0.20	0.22	0.25	0.28
	4.	0.50	0.43	0.64	0.57
Side Bending	1.	0.11	0.10	0.13	0.13
	2.	0.06	0.07	0.08	0.09
	3.	0.53	0.45	0.67	0.60
	4.	0.15	0.15	0.18	0.19
Axial Rotation	1.	0.64	0.66	0.78	0.83
	2.	0.19	0.17	0.22	0.21
	3.	0.15	0.16	0.18	0.20
	4.	0.34	0.29	0.43	0.38

Table 6-3 - Pin bending in the cranio-caudal direction during various ranging exercises in four subjects: calculated maximal angular and linear errors for segmental motion measurements using two different beam-bending models (Appendix).

6.1.3 Comparison To Cineradiography

Two subjects performed the exercises while simultaneous cineradiography and electromagnetic measurements were recorded to directly compare the results obtained with the electromagnetic tracking method with another independent method. The electromagnetic measurements for lateral bending were compared with the measurements made on the films by two independent orthopaedic surgeons and an interclass correlation was performed to compare the three results.

The inter-observer difference (mean = 1.01 degrees) was higher than the overall angular error (mean = 0.42 degrees) calculated from the tracking system. Calculating the interclass correlation coefficient (ICC) for the two observers and the two methods, the agreement between the two methods (ICC = 0.81) was slightly higher than the agreement between the two observers (ICC = 0.74). This is a direct reflection of the inaccuracy of identifying the same anatomical landmark on different films.

6.2 Computer Animation

The GE Signa 5.X MR data files can be successfully converted to the MINC storage format and the AVS module is able to interpret these image volume files and their header information. The segmentation process proved to be the most challenging to solve. The seeded region growing algorithm failed due to noise which allowed the region to expand beyond the correct boundaries of the surface. The simple manual tracing method is more robust, yet requires much more human interaction. Conversion of the segmented data to a geometrical poly-triangle mesh description is accomplished using a module provided with the AVS distribution. Control over the resolution of the mesh is available to the operator and the limitation of the computer hardware quickly becomes apparent if geometries are not down-sampled before being animated. This is not a problem at this point in time, but if finer surface detail is needed--to study the facet joint kinematics for instance--then the animation will have to be processed by a more performant computer.

6.2.1 Explanation of Video

Included with this submission is a short video demonstration of the animation of the L3-L4 vertebral segment of one subject. Only two vertebrae are shown, but the method is capable of animating all three instrumented vertebrae, provided the computer is fast enough to render a smooth animation and has enough RAM to hold the data structures of all the vertebrae. As well, a low resolution mesh was used to represent the vertebrae in the video because the animation frames needed to be transmitted over the network to a computer equipped with video output terminals. Even so, the quality of the surface is still good and the intuitive value of such an animation is excellent, but there are limitations to using this information for quantitative analysis.

7. Discussion & Conclusion

This project succeeded in developing the first reported method to directly study three-dimensional lumbar segmental kinematics. Similar invasive methods have been reported, however, none has previously combined a six degree of freedom measurement system, stereo radiographic calibration and MR image data from the same subject to measure and animate real segmental motion.

When describing the method's accuracy and reliability, a conservative approach was taken and the error estimates due to the dynamic tracking of the vertebrae and the error estimates due to pin deformations were added. The results are estimated angular errors for flexion/extension, side bending and axial rotation measurements as 0.44°, 0.49°, 0.38° respectively. The estimated linear errors for A/P shear, lateral shear and axial compression measurements are 0.57 mm, 0.75 mm, and 0.69 mm respectively. There is no inclusion of error due to bone deformation because of the difficulty in quantifying it.

The measurement error of this method is less those of non-invasive stereo radiography, but greater that those of stereo radiography using invasive placement of radio-dense markers. The great advantage of this method comes from its ability to accurately track motion in six degrees of freedom.

To date, 26 healthy subjects have undergone the *in-vivo* experiment. The method's invasiveness was well tolerated by the volunteers and the local anaesthesia kept the subjects sufficiently pain-free during the experiment. As well, the presence of the pins did not seem to alter their normal motion. Throughout the experiment a strict safety protocol was observed and we encountered no major complications.

Of the 26 original subjects, only 16 have undergone MR imaging so far. Currently, the process of converting the MR data to vertebral geometrical objects and finally integrating the kinematic data to create animated vertebral segments utilises two applications: one for the segmentation process and one for the integration of kinematic data and the display of the rendered animation. Considering the complication of the task at hand, the applications are relatively simple, and a deep understanding of the underlying process is not needed. Some training is required of course, and the quality of the segmentation is still a function of operator skill.

The addition of the 3-D animation can now be used as a tool to observe not only vertebral motion at the endplates, but to study the dynamics of facet motion, the mechanism of nerve root compression and

The next step in the continuation of this project would be to apply the method to a collective of patients with a specific pathology and compare the results with the healthy collective's data. As well, improvements to the segmentation algorithms could automate the MR data processing and the user interface could be unified into one tool that is easier to learn and use.

8. Appendix

8.1 Errors due to Pin Deformation

Two models were constructed to calculate the error due to pin bending:

Point Force Model: The relationship between the net vertical pin deflection (Y in Figure 8-1) at the location of the sensor and the radius of curvature (r) at the center of the strain gauges (x = z) is given by

$$Y = \frac{a^2(a+3L)}{6r(a-z)} \qquad \text{Equation A-1}$$

where the force F is applied at x = a, which is the distance between the spinous process and the skin, the angle of deflection (θ) is given by

$$\theta = \frac{a^2}{2r(a-z)} \qquad \text{Equation A-2}$$

Uniformly Distributed Load Model: If we assume a uniformly distributed force along the length of the pin between the spinous process and the skin (Figure 8-2), the relationship between the deflection (Y) and the radius of curvature (r) is given by

$$Y = \frac{a^3(4L - a)}{12r(a - z)^2}$$ Equation A-3

The angle of deflection (θ) is given by

$$\theta = \frac{a^3}{3r(a - z)^2}$$ Equation A-4

Calibration: During the strain gauge calibration, a force is applied to the pin using a micrometer (i.e. by increasing Y) at x = d, thus we use the point force model with a = d. We measure Y from the micrometer and the voltage (V) from the strain gauges. The relationship between Y and V has been found to be linear (i.e. $R^2 = 0.999$) for each of the strain gauges. Thus

$$Y = K \times V$$ Equation A-5

where K is a constant. Therefore from equations (A-1) and (A-5) we get

$$\frac{1}{r} = 3KV\left(\frac{d - z}{d^2(d + 3L)}\right)$$ Equation A-6

where **z**, **L**, and **d** are constants for each pin, and **K** is a constant found during each calibration. Thus we have linear relationship between 1/r and V.

Experiment: During the experiment, if we first assume *a point force at the skin*, the *angular error* (θ_1)from equations (A-2) and (A-6) is given by

$$\theta_1 = \frac{3a^2KV(d-z)}{2d^2(a-z)(d+3L)}\text{radians} \qquad \text{Equation A-7}$$

and the *linear error* (Y_1) from equations (A-1) and (A-6) is given by

$$Y_1 = \frac{a^2KV(d-z)(a+3L)}{2d^2(d+3L)(a-z)}\text{mm} \qquad \text{Equation A-8}$$

where **L, d, a** and **z** are constants for each pin, **K** is the calibration constant, and **V** is the voltage measured from the strain gauges during the experiment.

If the assumption of a *uniformly distributed load between the bone and skin* is used, the *angular error* (θ_2) from equations (A-4) and (A-6) is given by

$$\theta_2 = \frac{a^3KV(d-z)}{d^2(a-z)^2(d+3L)}\text{radians} \qquad \text{Equation A-9}$$

and the *linear error* (Y_2) from equations (A-3) and (A-6) is given by

$$Y_2 = \frac{a^3KV(d-z)(4L-a)}{4d^2(a-z)^2(d+3L)}\text{mm.} \qquad \text{Equation A-10}$$

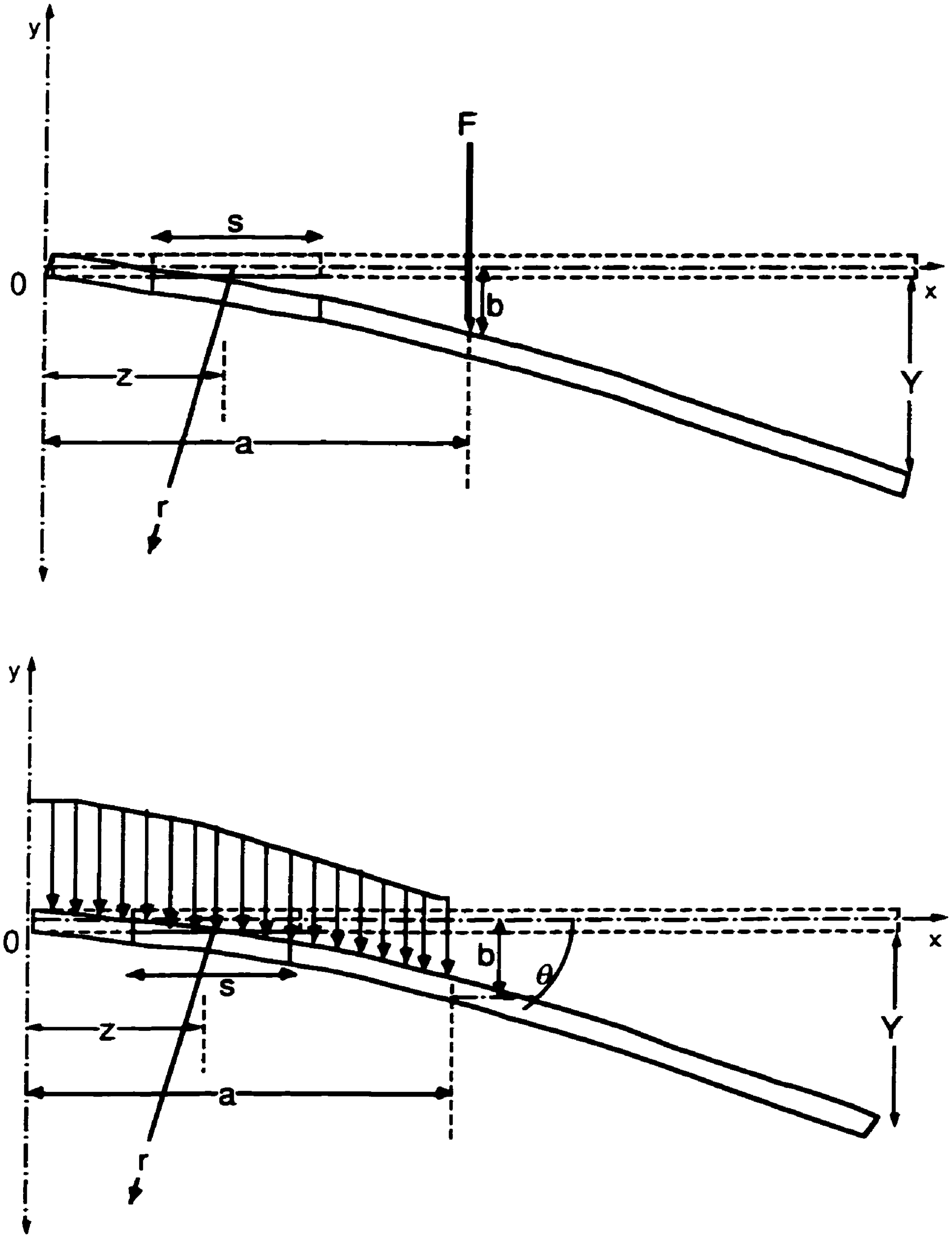

Figure 8-1 & 8-2 - Pin deformation schematics for the point force model (top) and the uniformly distributed load model (bottom)

9. References

[1] E. J. Nordby, "Epidemiology and Diagnosis in Low Back Injury," *Occup. Health and Saftey*, pp. 38-42, 1981.

[2] D. M. Spengler, S. J. Bigos, N. A. Martin, J. Zeh, L. Fisher, and A. Nachemson, "Back injuries in industry: a retrospective study. I. Overview and cost analysis," *Spine*, vol. 11, pp. 241-5, 1986.

[3] F. Biering-Sorensen, "Low back trouble in a general population of 30-, 40-, 50-, and 60-year-old men and women. Study design, representativeness and basic results," *Danish Medical Bulletin*, vol. 29, pp. 289-99, 1982.

[4] J. W. Frymoyer and B. W. Cats, "Predictors of low back pain disability," *Clinical Orthopaedics & Related Research*, 1987.

[5] V. K. Goel and J. N. Weinstein, *Biomechanics of the spine: Clinical and surgical perspective*. Boston: CRC Press, 1991.

[6] M. H. Pope and J. E. Novotny, "Spinal biomechanics," *J Biomech Eng*, vol. 115, pp. 569-74, 1993.

[7] M. G. Boocock, J. A. Jackson, A. K. Burton, and K. M. Tillotson, "Continuous measurement of lumbar posture using flexible electrogoniometers," *Ergonomics*, vol. 37, pp. 175-85, 1994.

[8] N. Paquet, F. Malouin, C. L. Richards, J. P. Dionne, and F. Comeau, "Validity and reliability of a new electrogoniometer for the measurement of sagittal dorsolumbar movements," *Spine*, vol. 16, pp. 516-9, 1991.

[9] J. W. Youdas, J. R. Carey, and T. R. Garrett, "Reliability of measurements of cervical spine range of motion--comparison of three methods," *Phys Ther*, vol. 71, pp. 98-104, 1991.

[10] J. Dillard, J. Trafimow, G. B. Andersson, and K. Cronin, "Motion of the lumbar spine. Reliability of two measurement techniques," *Spine*, vol. 16, pp. 321-4, 1991.

[11] K. Gill, M. H. Krag, G. B. Johnson, L. D. Haugh, and M. H. Pope, "Repeatability of four clinical methods for assessment of lumbar spinal motion," *Spine*, vol. 13, pp. 50-3, 1988.

[12] J. Cholewicki and S. M. McGill, "Lumbar posterior ligament involvement during extremely heavy lifts estimated from fluoroscopic measurements," *J Biomechanics*, vol. 25, pp. 17-28, 1992.

[13] S. Gracovetsky, M. Kary, S. Levy, R. Ben-Said, I. Pitchen, and J. Helie, "Analysis of spinal and muscular activity during flexion/extension and free lifts," *Spine*, vol. 15, pp. 1333-9, 1990.

[14] S. M. McGill, "A myoelectrically based dynamic three-dimensional model to predict loads on lumbar spine tissues during lateral bending," *J Biomechanics*, vol. 25, pp. 395-414, 1992.

[15] P. Wing, I. Tsang, F. Gagnon, L. Susak, and R. Gagnon, "Diurnal changes in the profile shape and range of motion of the back," *Spine*, vol. 17, pp. 761-6, 1992.

[16] M. A. Adams and P. Dolan, "A technique for quantifying bending moment acting on the lumbar spine in vivo," *J Biomechanics*, vol. 24, pp. 117-26, 1991.

[17] R. J. Hindle and M. J. Pearcy, "Rotational mobility of the human back in forward flexion," *Journal of Biomedical Engineering*, vol. 11, pp. 219-23, 1989.

[18] J. N. Nelson, R. P. Walmsley, and J. M. Stevenson, "Relative lumbar and pelvic motion during loaded spinal flexion/extension," *Spine*, vol. 20, pp. 199-204, 1995.

[19] M. J. Pearcy, "Twisting mobility of the human back in flexed postures," *Spine*, vol. 18, pp. 114-9, 1993.

[20] M. H. Pope, M. Svensson, H. Broman, and G. B. Andersson, "Mounting of the transducers in measurement of segmental motion of the spine," *J Biomechanics*, vol. 19, pp. 675-7, 1986.

[21] P. Roozmon, S. A. Gracovetsky, G. J. Gouw, and N. Newman, "Examining motion in the cervical spine. I: Imaging systems and measurement techniques," *J Biomed Eng*, vol. 15, pp. 5-12, 1993.

[22] I. A. F. Stokes and J. W. Frymoyer, "Relationship between movements of vertebrae and adjacent skin markers and sections of the back," Oxford Orthopaedic Engineering Center, Oxford 1977.

[23] G. G. Gregersen and D. B. Lucas, "An in vivo study of the axial rotation of the human thoracolumbar spine," *J Bone Joint Surg*, vol. 49A, pp. 247-62, 1967.

[24] R. M. Lumsden and J. M. Morris, "An in vivo study of axial rotation and immoblization at the lumbosacral joint," *J Bone Joint Surg*, vol. 50A, pp. 1591-602, 1968.

[25] R. Gunzburg, W. Hutton, and R. Fraser, "Axial rotation of the lumbar spine and the effect of flexion. An in vitro and in vivo biomechanical study," *Spine*, vol. 16, pp. 22-8, 1991.

[26] A. M. Kaigle, M. H. Pope, B. C. Fleming, and T. Hansson, "A method for the intravital measurement of interspinous kinematics," *J Biomechanics*, vol. 25, pp. 451-6, 1992.

[27] P. R. Dupuis, K. Yong-Hing, J. D. Cassidy, and W. H. Kirkaldy-Willis, "Radiologic diagnosis of degenerative lumbar spinal instability," *Spine*, vol. 10, pp. 262-76, 1985.

[28] J. Dvorak, M. M. Panjabi, D. G. Chang, R. Theiler, and D. Grob, "Functional radiographic diagnosis of the lumbar spine. Flexion-extension and lateral bending," *Spine*, vol. 16, pp. 562-71, 1991.

[29] F. Knutsson, "The instability associated with disc degeneration in the lumbar spine.," *Acta Radiol*, vol. 25, pp. 293, 1944.

[30] M. Panjabi, D. Chang, and J. Dvorak, "An analysis of errors in kinematic parameters associated with in vivo functional radiographs," *Spine*, vol. 17, pp. 200-5, 1992.

[31] M. M. Panjabi, V. K. Goel, S. D. Walter, and S. Schick, "Errors in the center and angle of rotation of a joint: an experimental study," *J Biomech Eng*, vol. 104, pp. 232-7, 1982.

[32] H. Van Mameren, H. Sanchez, J. Beursgens, and J. Drukker, "Cervical spine motion in the sagittal plane. II. Position of segmental averaged instantaneous centers of rotation--a cineradiographic study," *Spine*, vol. 17, pp. 467-74, 1992.

[33] T. H. Olsson, G. Selvik, and S. Willner, "Mobility in the lumbosacral spine after fusion studied with the aid of roentgen stereophotogrammetry," *Clin Orthop Rel Res*, vol. 129, pp. 81-90, 1977.

[34] M. J. Pearcy and M. W. Whittle, "Movements of the lumbar spine measured by three-dimensional X-ray analysis," *J Biomed Eng*, vol. 4, pp. 107-12, 1982.

[35] C. H. Suh, "The fundamentals of computer aided X-ray analysis of the spine," *J Biomechanics*, vol. 7, pp. 161-9, 1974.

[36] N. Egund, T. H. Olsson, H. Schmid, and G. Selvik, "Movements in the sacroiliac joints demonstrated with roentgen stereophotogrammetry," *Acta Radiol*, vol. 19, pp. 833-46, 1978.

[37] S. Lee, K. G. Harris, J. Nassif, V. K. Goel, and C. R. Clark, "In vivo kinematics of the cervical spine. Part I: Development of a roentgen stereophotogrammetric technique using metallic markers and assessment of its accuracy," *J Spinal Disord*, vol. 6, pp. 522-34, 1993.

[38] R. H. Brown, A. H. Burstein, C. L. Nash, and C. C. Schock, "Spinal analysis using a three-dimensional radiographic technique," *J Biomechanics*, vol. 9, pp. 355-65, 1976.

[39] I. A. Stokes, D. G. Wilder, J. W. Frymoyer, and M. H. Pope, "1980 Volvo award in clinical sciences. Assessment of patients with low-back pain by biplanar radiographic measurement of intervertebral motion," *Spine*, vol. 6, pp. 233-40, 1981.

[40] M. M. Panjabi, A. A. White III, "Clinical Biomechanics of the Spine, 2nd ed.," J.B. Lippincott Company, Philadelphia, 1990.

[41] R. Deklerck, J. Cornelis, and M. Bister, "Segmentation of medical images," Image & Vision Computing, vol. 11, pp. 486-503., 1993.

[42] Bezdek Jc, Hall Lo, and Clarke Lp, "Review of MR image segmentation techniques using pattern recognition. [Review]," Medical Physics, vol. 20, pp. 1033-48, 1993.

[43] E. A. Ashton, M. J. Berg, K. J. Parker, J. Weisberg, C. W. Chen, and L. Ketonen, "Segmentation and features extraction techniques, with applications to biomedical images," IEEE International Conference on Image Processing, vol. 3, pp. 726-739, 1994.

[44] J. L. Lee and J. J. Rodriguez, "Edge-based segmentation of 3-D magnetic resonance images," IEEE International Conference on Image Processing, vol. 1, pp. 876-880, 1994.

[45] Z. Liang, "Tissue classification and segmentation of MR images," IEEE Engineering in Medicine & Biology Magazine, vol. 12, pp. 81-85., 1993.

[46] Dhawan Ap and Arata L, "Segmentation of medical images through competitive learning," Computer Methods & Programs in Biomedicine, vol. 40, pp. 203-15, 1993.

10. Glossary

a, e, r - angular offsets in a CST (azimuth, elevation, roll)

AVS - Application Visualization System by Advanced Visual Systems Inc.

Bo - External magnetic field in the Larmor equation.

CSF - Cerebral Spinal Fluid

CS - Coordinate System

CST - Coordinate System Transformation

CT - Computed Tomography

DAT - Digital Audio Tape

DOF - Degree of Freedom

FID - Free-induction decay signal.

LabView - Graphical Development Environment by National Instruments

LBD - Low Back Disorders

MRI - Magnetic Resonance Imaging

RF - Radio Frequency

RMS - Root Mean Squared

ROM - Range of Motion

SEU - Fastrak System Electronics Unit

T1 - longitudinal relaxation time constant

T2 - transverse relaxation time constant

T2* - decay constant that includes the effects of static field inhomogeneity

TE - Time to Echo during an acquisition sequence

TR - Repetition Time during an acquisition sequence

ω - Larmor Frequency

γ - Gyromagnetic ration (42.58MHz/T for the hydrogen molecule).

x, y, z - linear offsets in a CST